University of Cambridge
Department of Engineering

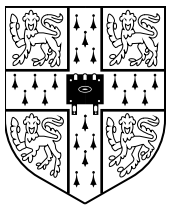

Analysis of Wrinkle Patterns in Prestressed Membrane Structures

Dissertation submitted to the University of Cambridge

for the Degree of Master of Philosophy

by

Yew Wei WONG

Wolfson College

August 2000

Acknowledgements

The work described in this dissertation was carried out by the author in the Department of Engineering, University of Cambridge from October 1999 to August 2000.

First, my heartfelt thanks to my supervisor, Dr. Sergio Pellegrino for his constant guidance and encouragement throughout the research. His unwaning enthusiasm and keen insight have been a main source of inspiration. Also, I should thank my adviser, Professor C. R. Calladine, *FRS*, for his interest in my work and for the many useful suggestions relating to the analytical solutions and experimental work.

I would like to thank all the members in the Deployable Structures Group and Structure Research Group for their constructive suggestions and friendships. In particular to Jason Lai for his help in Matlab programming and to Andrew Lennon and Gunnar Tibert for proof reading this dissertation and correcting my English. Also, excellent technical support and assistance was received from Mr. Roger Denston and Mr. Peter Knott.

This study was jointly funded by the Cambridge Commonwealth Trust (CCT), European Space Agency (ESA) and also from my parents. All funding received is gratefully acknowledged.

Finally, special thanks to those who are the most important to me, my parents, sister and brother for their support without which this work would not have been possible.

Declaration

The author declares that, except for commonly understood and accepted ideas, or where specific reference is made to the work of other authors, the contents of this dissertation are his own work and include nothing that is the outcome of work done in collaboration. This dissertation has not been previously submitted, in part or in whole, to any University or Institution for any degree, diploma or other qualification. This dissertation is presented in 70 pages and contains approximately 14000 words, including bibliography.

Yew Wei Wong

Abstract

Structural wrinkling is a common phenomenon found in thin membranes when subjected to different loading and boundary conditions. There are plans for increased use of prestressed membrane structures in space missions, for example the Next Generation Space Telescope solar shield and some Space Based Radar systems. These structures are often partially wrinkled and the formation of wrinkles drastically alters load paths and structural stiffness within the membrane. A better understanding of the effects of wrinkles on the structural performance and stability of these structures is essential and desirable.

This dissertation presents two different approaches, both applying a commercial non-linear finite element code (ABAQUS) to analyse and predict the wrinkle patterns and its associated wrinkle parameters. These finite element models are based on observations made in two preliminary experiments.

The first approach used the commonly available membrane element incorporating no-compression material behaviour to simulate the wrinkling condition in a two-dimensional manner. A simple analytical solution was developed and implemented in a Matlab script to predict the out-of-plane deformation of membrane structures.

The second approach used shell elements in a buckling prediction analysis to give the initial imperfection that, once introduced in the structure, would induce the formation of wrinkles. This analysis predicted the final wrinkle shapes in addition to an estimate of the out-of-plane deformation of the membrane. Compressive principal stresses were allowed to develop in this model.

This study showed that the finite element analysis can provide good estimates of the wrinkling behaviour in a membrane subjected to tension and shear with free or clamped boundary conditions. The results from the analysis displayed good agreement with those observed in the experiments.

An analytical wrinkle model was proposed, based on the assumption that a membrane is able to resist a small compressive stress once it has wrinkled. This model was developed for the case of a long membrane subjected to pure shear and clamped at the upper and bottom edges, by using the static equilibrium equation of the membrane in the deformed configuration. This solution was then

compared to an alternative analytical solution based on strain energy. Identical solutions were found using these two analytical methods and the results predicted agreed with those observed in the experiments.

Keywords: wrinkling; membrane; tension field; finite elements; no-compression material; geometrical non-linear; eigenvalue buckling analysis; critical wrinkling stress; wrinkle patterns; wavelength; amplitude.

Contents

Acknowledgements i

Declaration ii

Abstract iii

List of Tables viii

List of Figures xi

1 Introduction and Review of Literature 1

1.1 Introduction 1

1.2 Wrinkling Phenomenon 1

1.3 Review of Literature 4

1.3.1 Tension Field Theory 4

1.3.2 Stein-Hedgepeth Theory 7

1.3.3 Critical Compressive Stress Theory 9

1.3.4 Numerical Methods in Wrinkling Analysis 13

1.3.5 Wrinkling Criterion 14

1.4 Scope and Layout of the Dissertation 15

2 Experimental Observations 17

2.1 Introduction 17

2.2 Square Membrane Model 17

2.2.1 Observations 18
2.3 Membrane Model Subjected to Shear 20
2.3.1 Observations 21

3 Finite Element Analysis—No-compression Material Model 25
3.1 Element type 25
3.1.1 Geometric Non-linearity 26
3.1.2 No-compression Material 26
3.1.3 Artificial Stiffness 27
3.1.4 Strain Energy Stabilisation 27
3.2 Square Membrane Analysis 28
3.3 Wrinkling Program 29
3.3.1 Algorithm 31
3.3.2 Simple Wrinkle Model 31
3.4 Inflated Party Balloon 35
3.4.1 Discussion 36

4 Finite Element Analysis—Non-linear Shell Model 39
4.1 Prediction of Failure Modes 39
4.1.1 Introduction of Geometric Imperfections 40
4.2 Rectangular Membrane Model 41
4.2.1 Analysis 41
4.3 Discussion 42
4.3.1 Meshing 42
4.3.2 Imperfection Sensitivity 45
4.3.3 Comparison to Mansfield Model 47

5 Analytical Solution 51
5.1 Analysis 51
5.1.1 Membrane Equilibrium Approach 54

5.1.2 Strain Energy Approach 56
5.1.3 Prediction of Wrinkle Parameters 57
5.2 Comparison with Experiments Results 58
5.3 Discussion 62

6 Conclusions **64**
6.1 Discussion 64
6.1.1 Use of Finite Elements in Wrinkling Analysis 64
6.1.2 The Analytical Approach 65
6.2 Future work 66

Bibliography **68**

List of Tables

2.1 Summary of observations for different materials at 8 mm displacement. 23

3.1 Comparisons between the physical and FE model. 36

4.1 Comparisons between three different mesh densities for the FE model. 43

4.2 Comparisons between different magnitude of imperfections with respect to the maximum amplitude obtained in the buckling analysis. 45

5.1 Experimental and analytical results for Kapton membrane of thickness 0.035 mm. 59

5.2 Experimental and analytical results for Mylar membrane of thickness 0.05 mm. 60

5.3 Experimental and analytical results for a rubber membrane of thickness 1 mm. 61

5.4 Comparisons between experimental and analytical solution for three materials. 62

List of Figures

1.1 Solar sail with wrinkles radiating out from the corners. 2

1.2 Wrinkles occurring along (a) the outer edge and (b) the seams of the reflector. 2

1.3 Slotted waveguide: wrinkles are found along the edges and between seams. 3

1.4 Scale model of Synthetic Aperture Radar (SAR) (Watt, 2000): wrinkles may be observed at the corners and along the edges of the surface. 3

1.5 An arbitrary membrane with two adjacent tension rays. 5

1.6 Equilibrium of two adjacent tension rays. 6

1.7 Bending experiment and closed-form results using the Stein-Hedgepeth theory. 8

1.8 Rotation experiment and closed-form results using the Stein-Hedgepeth theory. 9

1.9 Blanket suspended in gravitational field and the equilibrium of a blanket element. 10

1.10 Various components in the third tension strip. 11

1.11 Experimental observations in the blanket. 13

2.1 Wrinkle observation experiment. 18

2.2 Wrinkle observed in the experiment. 19

2.3 Bottom frame and the components of the model. 20

2.4 Frame model. 21

2.5 Simple test rig for the frame model. 22

2.6 Wavelengths at 4 mm were larger than at 8 mm. 23

2.7 Final wrinkle patterns for different materials, at 8mm displacement. 24
2.8 Plots of wavelength against displacement for different materials. . 24

3.1 FE model of square membrane. 28
3.2 Wrinkling analysis using no-compression material. 30
3.3 Wrinkle pattern from wrinkling program. 32
3.4 Simple parabola wrinkle model, section A-A of Figure 3.3(b) . . . 33
3.5 Parabola 33
3.6 Out of plane deformation using simple wrinkle model. 35
3.7 FE model for party balloon. 36
3.8 Comparison between FE model and physical model. 37
3.9 Contour plot of major principal stress in the inflated balloon. . . . 38

4.1 First two eigenmodes predicted by buckling analysis, (a) first mode shape and (b) second mode shape 42
4.2 Finite Element Model. 43
4.3 Definition of wrinkles from contour plot of out-of-plane deformation. 44
4.4 Contour plot of major principal stress. 44
4.5 Final wrinkle pattern. 44
4.6 Principal stresses variation at mid-plane of the membrane. 45
4.7 Comparison between wavelength obtained from experiment and finite element analysis for Mylar membrane. 46
4.8 Boundary conditions used to determine the function, F. 47
4.9 Tension ray lines from FE analysis. 49
4.10 Comparison of tension ray lines from Mansfield (1968) and FE model. 49

5.1 Long, flat isotropic membrane clamped to rigid upper and lower edges 52
5.2 Membrane subjected to uniform forces at edges. 52
5.3 Wrinkle pattern in a membrane subjected to pure shear. 54
5.4 Equilibrium state in a tension strip 55

5.5 Comparison between experimental and analytical solution for Kapton membrane. 59

5.6 Comparison between experimental and analytical solution for Mylar membrane. 60

5.7 Comparison between experimental and analytical solution for Rubber membrane. 61

5.8 Plot to verify the relationship between wavelength and displacement. 63

Chapter 1

Introduction and Review of Literature

1.1 Introduction

There is an increasing number of space missions in which it is proposed to use membrane structures with a wide variety of shapes and sizes. Most of these structures require high accuracy; hence the use of a prestressed surface is envisaged. The solar shield for the Next Generation Space Telescope (NGST), proposed Space Based Radar (SBR) satellites (Adler et al., 2000) and the inflatable antenna (Bernasconi and Rits, 1990; Grossman, 1998; Kato, 1988; Kato, 1989) and also future solar arrays and solar sails are examples of such membrane structures. Most of the prestressed membrane structures involved in these missions are partially wrinkled in their operational configuration; see Figures 1.1–1.4. The occurrence of wrinkles may cause adverse effects on the overall structural stability of these structures. It also affects the intended performance of structures such as reflectors which require high geometrical accuracy for the membrane surface (Lai, 1997). Wrinkling is currently regarded as a mode of failure for a high-precision membrane reflector. Therefore, it is important to study and understand the behaviour of these structures when wrinkling occurs, and to develop a validated wrinkling analysis method.

1.2 Wrinkling Phenomenon

Wrinkling is a phenomenon usually associated with the deformation of a thin membrane surface when subjected to compressive stresses. A membrane is usually assumed to have no bending stiffness, hence compressive stresses cannot exist, i.e. wrinkling occurs immediately. A surface subjected to a purely tensile stress state

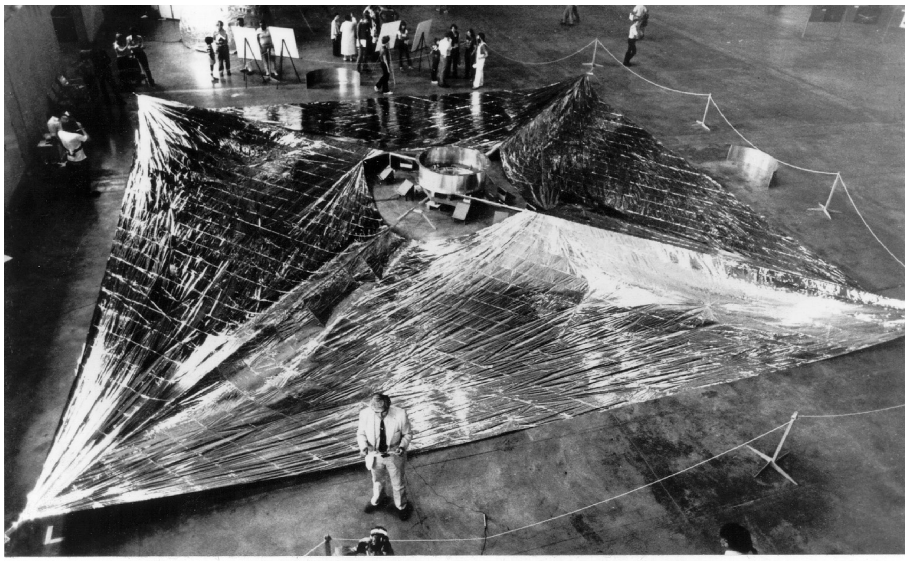

Figure 1.1: Solar sail with wrinkles radiating out from the corners.

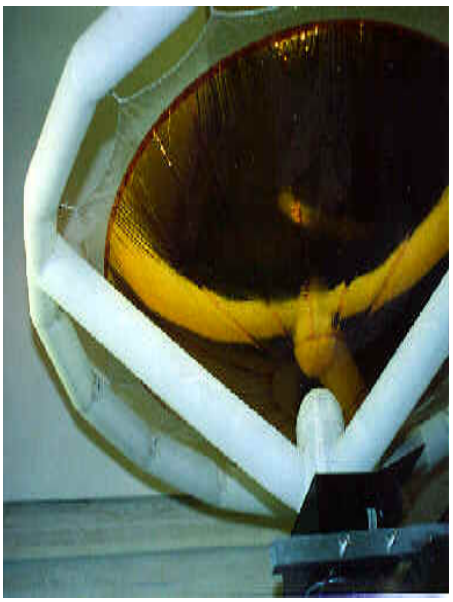

(a) Microspacecraft antenna.

(b) Inflatable antenna experiment

Figure 1.2: Wrinkles occurring along (a) the outer edge and (b) the seams of the reflector.

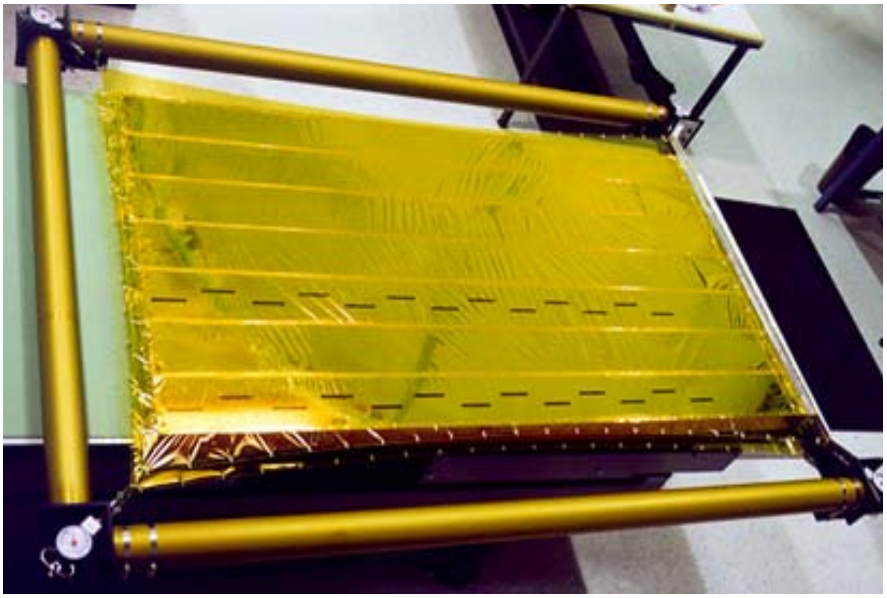

Figure 1.3: Slotted waveguide: wrinkles are found along the edges and between seams.

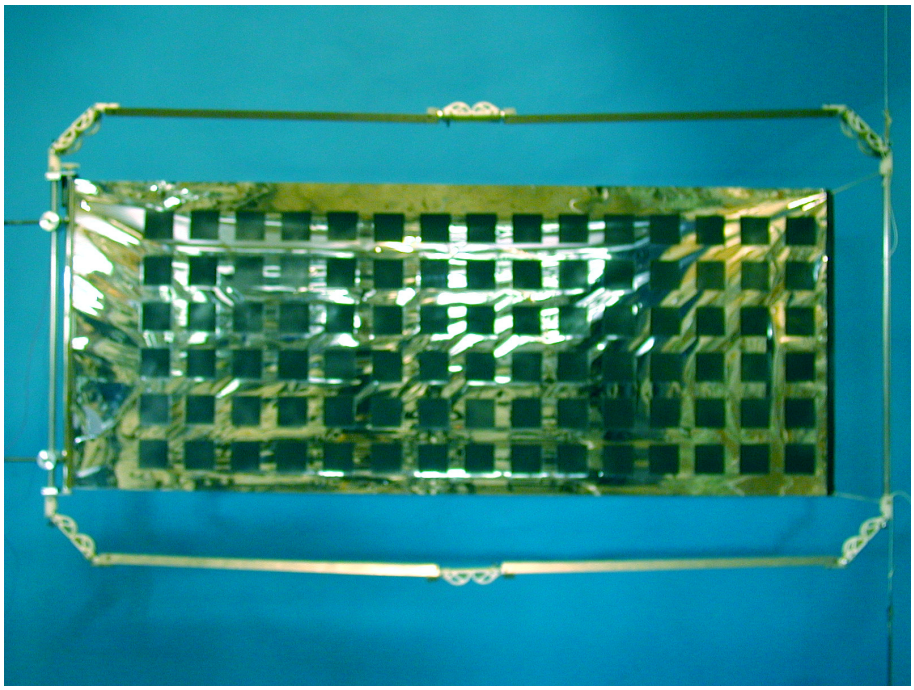

Figure 1.4: Scale model of Synthetic Aperture Radar (SAR) (Watt, 2000): wrinkles may be observed at the corners and along the edges of the surface.

is said to be free from wrinkles but often wrinkles can form due to the in-plane components of the load in the structure.

Generally there are two types of wrinkles, namely structural and material wrinkles. Structural wrinkles are the out-of-plane deformation due to localised buckling of the membrane when subjected to a compressive stress. The size, wavelength and the direction of these wrinkles varies depending upon the magnitude of the applied loads and boundary conditions. Structural wrinkles are not permanent deformations as they disappear with the removal of the applied loads. Material wrinkles are permanent out-of-plane deformations due to material and manufacturing imperfections, as well as the high localised strains induced by packaging of the material when it is folded in a tight radius (Murphey, 1998). This study concentrates on structural wrinkles since they may be eliminated through careful analysis and design of the structures.

1.3 Review of Literature

A number of theoretical approaches (Reissner, 1938; Stein and Hedgepeth, 1961; Mansfield, 1968; Rimrott and Cvercko, 1985; Pipkin, 1986) have been developed to deal with wrinkling problems, particularly in determining the wrinkled regions in thin membranes. However, this phenomenon has been treated as a plane stress problem.

1.3.1 Tension Field Theory

Tension field theory describes the state of stress in a membrane when its boundaries are stretched and displaced causing wrinkling in the membrane. This theory was first introduced by Wagner (1929), to estimate the maximum shear load that can be carried by a thin metal web in an I or box girder. The load required to fail the structure was found to be several times higher than the initial load that caused wrinkles to form in the thin web, provided the loading and boundary conditions remained the same after the formation of the first wrinkle. Later, the original solution based on lengthy geometrical considerations was simplified and the fundamental equations of the theory were derived by Reissner (1938). Mansfield (1968) introduced the idea of linking the principle of maximum strain energy to the membrane geometry through a coordinate system related to the tension ray[1] distribution. The strain energy used in tension field theory can be replaced by a suitable relaxed energy density according to Pipkin (1986) and consequently incorporating this theory into the ordinary elastic membrane theory. A summary of the general tension field theory is presented below.

[1]The line of principal tensile stress.

Analysis

Consider an initially flat membrane of any shape and stiffness which is subjected to given planar displacements at its boundaries. A tension field is assumed to be generated over the membrane due to this boundary condition. The primary objective in tension field theory is to determine the orientation of the tension rays in a highly wrinkled state of the membrane.

The strain energy in the membrane is due only to the tensile stresses, along the tension rays, since there are no direct and shear stresses across adjacent rays. Mansfield postulated that the true distribution of tension rays maximises this tensile strain energy, i.e. Principle of maximum strain energy.

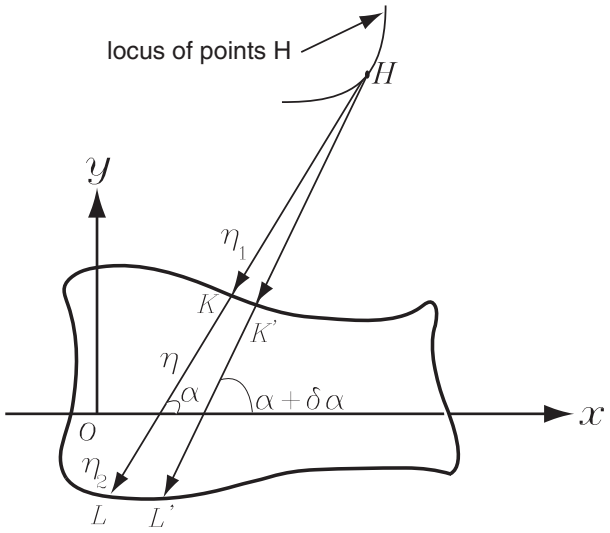

Figure 1.5: An arbitrary membrane with two adjacent tension rays.

A membrane of constant thickness, t, with reference axis ox is shown in Figure 1.5. Two adjacent tension rays denoted by LK, $L'K'$ intersect the x-axis at angles $\alpha, \alpha + \delta\alpha$ and meet at the point H. A general point in the membrane is defined by α and η, where η is the distance along the tension ray; it is a function of α and x. Maintaining equilibrium along the tension ray requires the continuity of the tensile load carried between adjacent rays, with the assumption that there is no stress across the rays as shown in Figure 1.6, we obtain

$$\eta\sigma_\eta = \text{constant} \tag{1.1}$$

where σ_η is the direct stress along a ray.

The integral of the strain ϵ_η, along line LK is equal to the change in length of LK and denoted by $\triangle_\alpha$; it depends on the given boundary displacements.

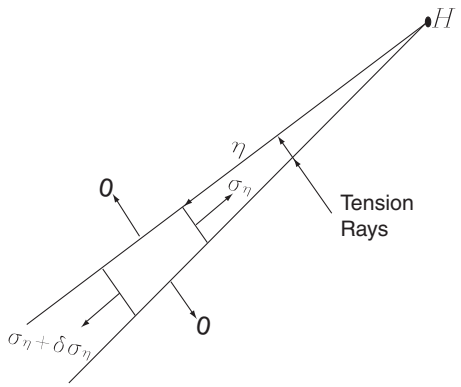

Figure 1.6: Equilibrium of two adjacent tension rays.

Therefore, the constant in Equation (1.1) can be identified and

$$\epsilon_\eta = \frac{\triangle_\alpha}{\eta\left(\ln\frac{\eta_2}{\eta_1}\right)} \tag{1.2}$$

where η_1 and η_2 are the boundary values of η, as shown in Figure 1.5. The strain energy in the membrane can be determined by integrating over an elemental slice bounded by two adjacent rays.

$$\begin{aligned} U &= \frac{1}{2}Et\int\int\epsilon_\eta^2 \mathrm{dA} = \frac{1}{2}\mathrm{Et}\int\int_{\eta_1}^{\eta_2}\epsilon_\eta^2\eta\mathrm{d}\eta\mathrm{d}\alpha \\ &= \frac{1}{2}\int F\mathrm{d}\alpha \end{aligned} \tag{1.3}$$

where

$$F = \frac{\triangle_\alpha^2}{\int_{\eta_1}^{\eta_2}\frac{1}{\eta Et}\mathrm{d}\eta} \tag{1.4}$$

The value of η on the x-axis can be determined by geometrical considerations,

$$\eta_x = \pm\left(\frac{\mathrm{d}x}{\mathrm{d}\alpha}\right)\sin\alpha \tag{1.5}$$

where the sign of Equation (1.5) depends on the position of point H relative to the x-axis. The relationship between α and x is determined by maximising U, therefore the general equation is

$$x''F_{x'x'} + x'F_{xx'} + F_{\alpha x'} - F_x = 0 \tag{1.6}$$

where $x' = \mathrm{d}x/\mathrm{d}\alpha$, $x'' = \mathrm{d}^2x/\mathrm{d}\alpha^2$, $F_x = \partial F/\partial x$, etc. Hence, F is a function of the variables α, x and x'. Note that if F does not contain x explicitly, Equation (1.6) can be integrated once to give

$$F_{x'} = \text{constant} \tag{1.7}$$

From Equations (1.1)–(1.7), it is seen that the determination of the distribution of tension rays is based solely on the displacement components along the tension rays. This relationship is used to determine the stress distribution in the membrane.

Note that the theory is valid only if

$$\triangle_\alpha > 0; \quad \epsilon_\alpha + \nu\epsilon_n \leqslant 0 \tag{1.8}$$

If the boundary of a membrane is straight and the number of free edges is restricted to two or less, the tension field in this state consists primarily of tension at 45°. The membrane bending stiffness and the in-plane compressive stresses are negligible in this theory.

Mansfield's tension field theory extended the general equations developed above to the study of the membranes with different strip lengths and boundary conditions subjected to shear. Also, membranes with different shapes and material properties, e.g. annular membranes and anisotropic membranes, were investigated. There were also experimental studies to verify the theory. Details of these studies can be found in Mansfield (1968) and Mansfield (1970).

1.3.2 Stein-Hedgepeth Theory

This theory, generally known as wrinkling theory (Stein and Hedgepeth, 1961), was developed specifically to analyse partly wrinkled membranes and it is applicable to more general problems.

The basic assumptions made in the theory are:

1. Compressive stresses are eliminated completely by the formation of wrinkles. Therefore, the minor principal stress is non-negative everywhere in the membrane.

2. The troughs and crests of wrinkles run in the directions of the local major principal axis.

3. The load in the wrinkled regions is carried only by the wrinkles in the directions of the troughs and crests. Hence, the minor principal stresses in the wrinkled region (perpendicular to the load paths) are zero.

A modified theory was derived from the linear elastic, isotropic plane stress theory based on the assumptions given above. The wrinkling theory assumes that there are two types of regions in a partly wrinkled membrane, namely taut and wrinkled.

Membranes behave linear elastically in the taut regions. In wrinkled regions a modified set of relationships using a variable Poisson's ratio (due to the overcontraction caused by the wrinkles) determines the membrane behaviour. The variable Poisson's ratio must match the material's Poisson's ratio at the boundaries between wrinkled and taut regions. The minor principal stresses must be zero for both regions. Stein and Hedgepeth used the theory to produce closed-form solutions for simple structures, such as a pressurised Mylar cylinder in bending, see Figure 1.7, and a stretched circular Mylar sheet attached to a rigid hub that is rotated, see Figure 1.8. Their solutions were verified experimentally.

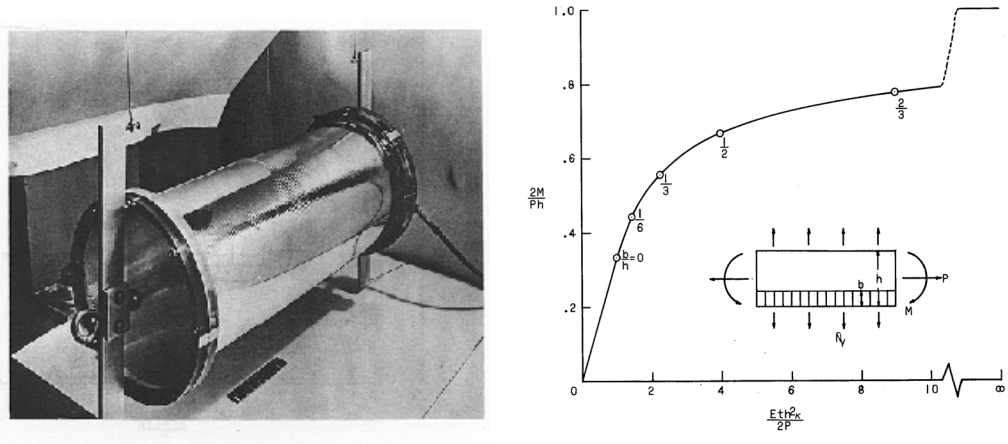

(a) Bending of Mylar cylinder experiment.

(b) Closed-form results.

Figure 1.7: Bending experiment and closed-form results using the Stein-Hedgepeth theory.

Detailed experimental studies on the Stein-Hedgepeth theory were done by Mikulas (1964), who analysed the stretched circular membrane and verified the results with an accurate experiment.

As discussed above, these theories only apply to 2-D problems. They are used to determine the regions of a membrane that wrinkle, the pattern those wrinkles take, the resulting stress field and load paths. They cannot be used to determine the out-of-plane wave shape produced by wrinkles, i.e. amplitude and wavelength.

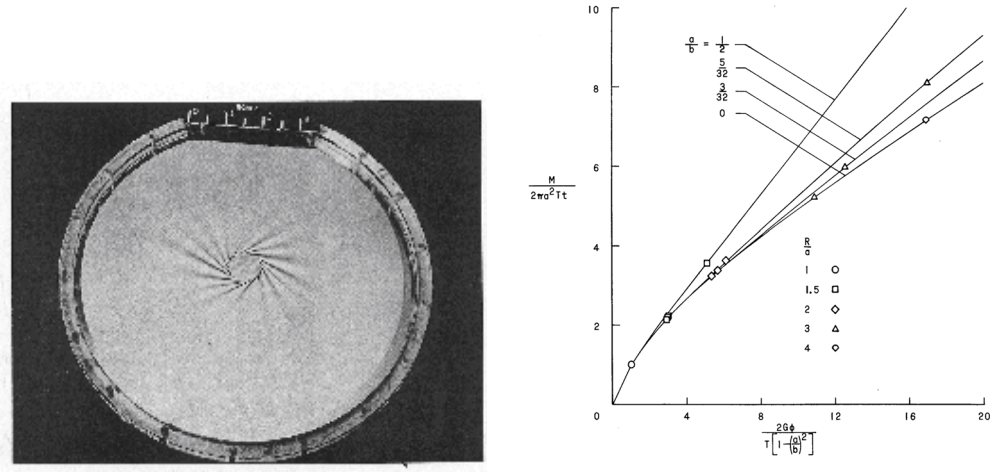

(a) Stretched circular membrane experiment.

(b) Closed-form results.

Figure 1.8: Rotation experiment and closed-form results using the Stein-Hedgepeth theory.

1.3.3 Critical Compressive Stress Theory

In both the tension field and the Stein-Hedgepeth theory, the bending stiffness in the membrane is neglected and the wrinkle only carries load in the direction of the major principal tensile stress, the body forces in the membrane being ignored.

The effect of in-plane body compression to the wrinkling of a thin membrane was investigated by Rimrott and Cvercko (1985). The membrane was analysed as a "blanket" supported at two ends. A series of cosine-shaped wrinkle lines formed in the blanket due to gravitational force as shown in Figure 1.9.

Analysis

The cosine-shaped wrinkle boundary is represented by

$$y = a_i \cos \frac{\pi x}{l} \tag{1.9}$$

where a is the amplitude of the cosine curve, i corresponds to the wrinkle lines formed in the blanket, e.g. $i = 0$ in the lower boundary and $i = n$ for upper boundary if there are n numbers of wrinkles formed in the blanket.

The equilibrium of an element in the blanket is given as

$$\frac{\partial^2 y}{\partial x^2} \mp \gamma \frac{\partial y}{\partial H} = 0 \tag{1.10}$$

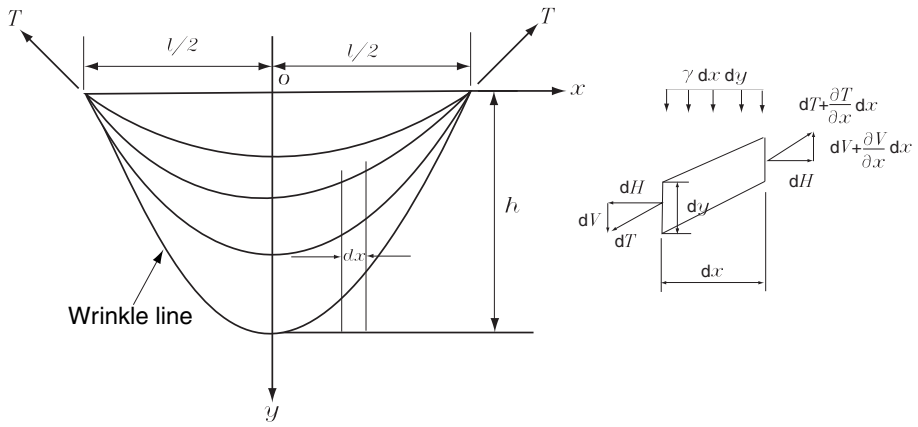

Figure 1.9: Blanket suspended in gravitational field and the equilibrium of a blanket element.

where γ is the specific weight of blanket, H is the horizontal force parameter. $\mp$ sign allows for cos-shape as well as cosh-shape tension lines. The stress component in x-direction is

$$\sigma_x = \mp \frac{\partial H}{\partial y} \tag{1.11}$$

In this study the tension field is subdivided into pre-wrinkling and post-wrinkling sections. The pre-wrinkling tension field is exactly the same as in the previous two theories, hence Equations (1.10) and (1.11) are satisfied. In the post-wrinkling condition, there is a small compressive stress caused by wrinkles in addition to the uniform tension stress distribution found in a tension strip.

Once a wrinkle has formed in the blanket, the lateral fallout caused by wrinkle leads to only a partial of the specific weight acting on the wrinkle line, from Figure 1.10

$$\begin{aligned} \frac{\gamma_f}{\gamma} &= \frac{a}{m} \\ \gamma_f &= \frac{a}{m}\gamma \end{aligned} \tag{1.12}$$

where γ_f is the partial specific weight and m is the amplitude of the center line in a tension strip. Substitute Equation (1.12) to Equation (1.10) to get

$$\frac{\partial^2 y}{\partial x^2} \mp \frac{a}{m}\gamma \frac{\partial y}{\partial H} = 0 \tag{1.13}$$

Note that the horizontal force component of the tension force, F, is required to be located along the center of each tension strip to maintain the equilibrium of each tension strip of finite size.

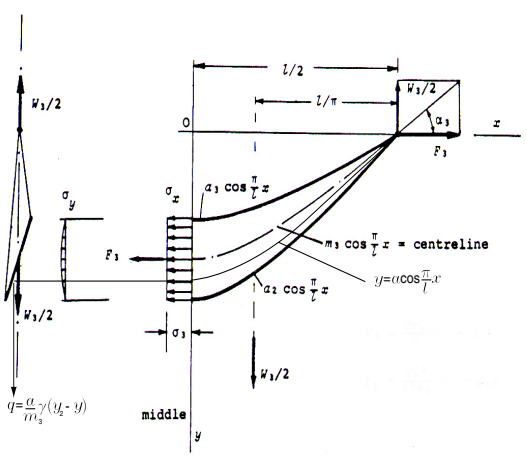

(a) Tension line, $y = a\cos\frac{\pi}{l}x$ in the third tension strip between wrinkle line 2, $a_2\cos\frac{\pi}{l}x$ and wrinkle line 3, $a_3\cos\frac{\pi}{l}x$.

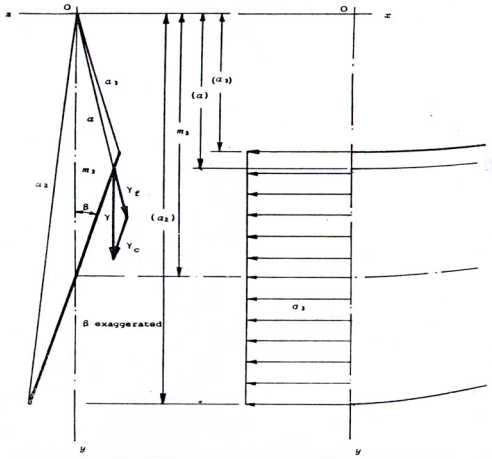

(b) Section through tension strip with lateral fallout.

Figure 1.10: Various components in the third tension strip.

By introducing a reduced distribution load, q, for an i^{th} tension strip in the blanket, as shown in Figure 1.10(a)

$$q = \frac{a}{m_i}\gamma\left(a_{i-1}\cos\frac{\pi x}{l} - y\right) \tag{1.14}$$

and let $\mathrm{d}H/\mathrm{d}y = -\sigma_{\mathrm{x}}$, from Equation (1.13), the governing equilibrium equation for the post wrinkling state can be written as

$$\frac{\partial^2 y}{\partial x^2} \pm \frac{q}{H} = 0 \tag{1.15}$$

Equation (1.15) also governs the shapes of the wrinkle lines and tension lines within each tension strip.

Figure 1.10(b) shows that the specific weight is no longer uniform, hence there is a supplementary specific force superimposed on the specific weight

$$\gamma_c = \gamma\left(1 - \frac{a}{m_i}\right) \tag{1.16}$$

and this force is produced by the in-plane body compression in y-direction. This stress is given by

$$\sigma_y = \int_y^{y_{i-1}} \gamma_c \mathrm{d}y = \gamma\left[\int_a^{a_i}\left(1 - \frac{a}{m_i}\right)\mathrm{d}a\right]\cos\frac{\pi x}{l} \tag{1.17}$$

After integration and expressing m_i in terms of a_i and a_{i-1}

$$\sigma_y = -\frac{\gamma}{2m_i}(a_{i-1} - a)(a - a_i)\cos\frac{\pi x}{l} \tag{1.18}$$

Note: $-$ sign indicates a compressive stress. The maximum compressive stress occurs along the centre line of the tension strip is

$$\max|\sigma_y| = \frac{\gamma}{2m_i}(a_{i-1} - m_i)(m_i - a_i)\cos\frac{\pi x}{l} = \frac{\gamma m_i}{2}\frac{(Q-1)^2}{(Q+1)^2}\cos\frac{\pi x}{l} \tag{1.19}$$

If there are n tension strips in a wrinkled region, then $Q = \sqrt[n]{a_0/a_n}$. Note that Equations (1.14)–(1.19) were derived for any tension strips in the blanket. However in Figure 1.10, $i = 3$, since third tension strip was chosen as an example.

If the blanket material has a critical wrinkling stress, σ_{cr}, from Equation (1.19), the following inequality must be satisfied throughout the wrinkled region

$$|\sigma_{\text{cr}}| \geq \frac{\gamma a_0}{4}\frac{(Q-1)^2}{Q(Q+1)} \tag{1.20}$$

This solution is verified with the experimental observations. The number of wrinkles increases as the specific weight of the material and the amplitude, a_0 of the blanket increases. Blanket with three and four wrinkles observed in this study (Rimrott and Cvercko, 1985) is shown in Figure 1.11.

Several assumptions were made in this study.

1. Bending stiffness is present in the membrane, with a finite number of wrinkles observed in the experiments. Hence a small compressive stress can be carried and is limited by a critical wrinkling stress.

2. The strain energy in tension is zero, see 4 below, and negligible in compression.

3. Bending strain energy is not negligible.

4. The tensile strength of a wrinkle is infinite and the material is assumed to be inextensional in tension.

This study shows the effects of the small bending stiffness that exists in the membrane; and the prediction of the formation of finite number of wrinkles and the corresponding amplitudes, when the membrane is subjected to the in-plane compression body force.

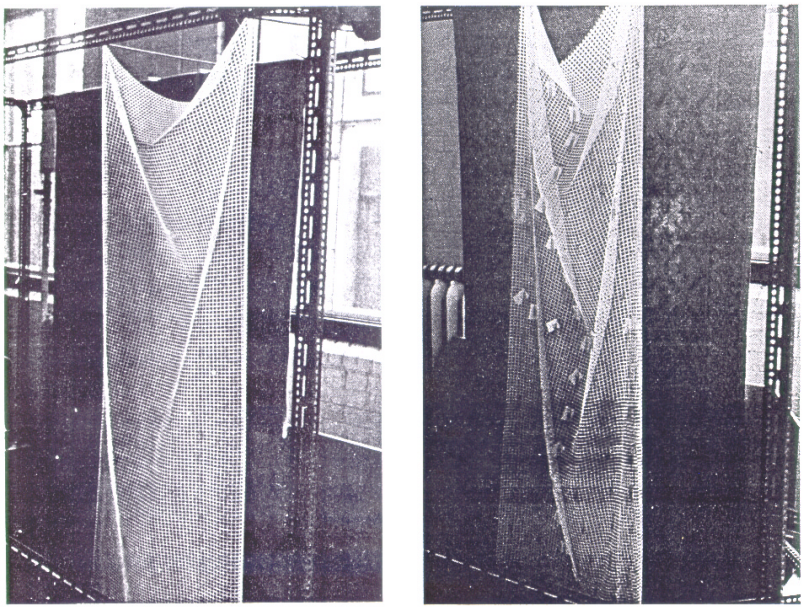

(a) Blanket with three wrinkles.

(b) Blanket with weights and four wrinkles.

Figure 1.11: Experimental observations in the blanket.

1.3.4 Numerical Methods in Wrinkling Analysis

The theoretical approaches in Sections 1.3.1–1.3.3 have only been applied to simple closed-form solutions. When non-uniform loading exists, closed-form solutions become very complicated. Therefore, adapting them to the Finite Element Method (FEM) solution becomes the only viable approach to analyse any type of prestressed membrane structures.

An iterative membrane properties (IMP) method based on the Stein-Hedgepeth theory was introduced by Miller et al. (1985) to recursively modify the properties of membrane elements to eliminate all the compressive stresses until only non-negative stresses are left in the membrane. Methods to implement the iterative scheme into existing total Lagrangian finite element codes for membranes have been proposed (Kang and Im, 1997; Adler et al., 2000). Also, a penalty parameter tension field algorithm was introduced to update the stress state using a non-linear dynamic FE code with curvilinear cable and membrane elements. Wrinkling in parachutes during deployment has been analysed by Liu et al. (1998). Non-linear geometrical FE analysis was used to solve an inflated air-bag problem by Contri and Schrefler (1988).

The FE numerical work presented above mainly concentrated on implementing a wrinkling condition to determine in-plane wrinkle patterns based on tension field

and wrinkling theory; hence 2-D membrane elements with no bending stiffness were employed. Due to the assumptions made, even by incorporating non-linear geometrical analysis, only the final wrinkled shape and in-plane wrinkled pattern could be obtained. Little attention was given to the prediction of the wrinkle parameters, i.e. the amplitude and the wavelength of the wrinkles.

Besides tension field theory, bifurcation buckling theory with the assumption that wrinkles are deformations associated with bifurcation buckling has been used in finite element analysis. Bifurcation analysis was used to investigate the wrinkling of a stretched circular membrane under in-plane torsion (Miyamura, 2000). The shape of the wrinkles was obtained precisely with this approach and the stress distributions obtained by the analysis were compared and show good correlation with the principal stresses measured in experiments. In this analysis, only geometrical stiffness was considered and hence the number of wrinkles and the amplitudes of the wrinkles were not compared. Elastic analysis is still an effective method to handle wrinkling problems since material nonlinearities and creep do not affect significantly the stress distributions.

1.3.5 Wrinkling Criterion

There are three different types of criteria to define the occurrence of wrinkling in a membrane, namely the principal stresses, $\sigma_{1,2}$ criterion, the principal strains, $\varepsilon_{1,2}$ criterion, and the combined criterion, including both principal stresses and principal strains.

For the wrinkling criteria based on principal stresses/strains the membrane is said to be in a *taut* condition when both the principal stresses/strains are positive, i.e. tensile. It is said to be *slack* if both principal stresses/strains are zero. In both the taut and slack states there is no wrinkling in the membrane. Thus, *wrinkling* occurs in the membrane when the minor principal stress/strain is zero and the major principal stress/strain is tensile.

For wrinkling based on the combined criterion, the membrane is in the *taut* condition when the minor principal stress is positive and it is *slack* when the major principal stress is zero. When the minor principal stress is negative and the maximum principal strain is positive, the membrane is *wrinkled* (Liu et al., 1998). Where $\sigma_{1,2}$ and $\varepsilon_{1,2}$ are the major and minor principal stresses respectively. The wrinkling criteria are summarised below:

a) Principal stress criterion

$$\begin{array}{llllll} \text{(i)} & \sigma_2 > 0, & \text{taut;} & & & \\ \text{(ii)} & \sigma_2 \leq 0 & \text{and} & \sigma_1 > 0, & \text{wrinkled;} & \\ \text{(iii)} & \sigma_2 \leq 0 & \text{and} & \sigma_1 \leq 0 & \text{slack.} & \end{array}$$

b) Principal strain criterion

(i)	$\varepsilon_2 > 0,$	taut;		
(ii)	$\varepsilon_2 \leq 0$	and	$\varepsilon_1 > 0,$	wrinkled;
(iii)	$\varepsilon_2 \leq 0$	and	$\varepsilon_1 \leq 0,$	slack.

c) Combined criterion

(i)	$\sigma_2 > 0,$	taut;		
(ii)	$\sigma_2 \leq 0$	and	$\varepsilon_1 > 0,$	wrinkled;
(iii)	$\sigma_1 \leq 0$	and	$\varepsilon_1 \leq 0,$	slack.

1.4 Scope and Layout of the Dissertation

The review of the literature shows that the existing studies on wrinkling have mainly considered the following points:

1. Analysis using tension field theory and Stein-Hedgepeth theory, treated the membrane as a 2-D problem.
2. Implementation of existing theories into FE codes to enable the analysis of more complex prestressed membrane structures with different loading and boundary conditions.
3. Experimental studies including measurement of stresses in the wrinkled membrane.
4. Use of bifurcation theory to treat the wrinkling as a buckling problem and to predict the wrinkle shapes.

However, determination of the details of the out-of-plane deformation produced by wrinkling, i.e. wavelength and amplitude and their relationships to the boundary and loading conditions applied to the membranes, have not been studied in detail. Also, two theories have been used in handling wrinkling problems, but the assumptions employed and results obtained by using these two approaches have not been compared and investigated.

In this study, we begin by treating the problem as two-dimensional. The analysis can be performed by incorporating the wrinkling theory in the finite element analysis of a thin membrane. This involves a geometrically non-linear finite element analysis of the membrane where wrinkled regions are modelled with no-compression material.[2] Then, the out-of-plane deformation of the wrinkle is

[2]The linear elasticity of the material is modified so that no compressive stress can be generated.

predicted using a simple analytical wrinkle model. In the second approach, thin shell element is employed to simulate wrinkling. Eigenvalue buckling analysis is then used to predict the wrinkling mode shapes. Geometrical imperfections are introduced to the initially flat mesh by extracting the eigenvectors from the mode shapes. The wrinkle pattern obtained in this approach is compared to a problem solved using tension field theory. Finally, an analytical solution is developed to predict the wrinkle wavelength in a membrane subjected to pure shear. The results obtained in the numerical and analytical analysis are compared to the observations from simple experiments.

The dissertation is presented as follows:

Chapter 2 presents a series of observations from two simple experiments, which inspire the following computational analysis.
Chapter 3 presents a wrinkling analysis using the finite element method by simulating the wrinkled region with no-compression material. A wrinkling program written in Matlab using a simple wrinkle model is used to predict the out-of-plane deformation for a particular example.
Chapter 4 presents the use of an initial eigenvalue analysis in a finite element simulation that models the membrane as a thin shell, to predict the wrinkling mode shapes in a membrane subjected to pure shear. The results from this approach are compared with results from Mansfield's tension field theory.
Chapter 5 presents a simple analytical approach to predict the wavelength of a membrane subjected to pure shear by using the static equilibrium equation of a membrane and strain energy approach.
Chapter 6 discusses the results from the analysis and the analytical approach and concludes the dissertation.

Chapter 2

Experimental Observations

2.1 Introduction

Wrinkling has been observed in many space structures, as shown in Figures 1.1–1.4. The formation of wrinkles in these structures may be due to the in-plane or normal[1] loading exerted on them during the process of packaging and handling, in the deployment stage and also during their service life (Rimrott and Cvercko, 1985; Greschik et al., 1998; Murphey, 1998). Two preliminary simple experiments have been devised to observe the wrinkle patterns and the associated wrinkle parameters when the structures are subjected to different loading and boundary conditions. These observations eventually formed the basis of the wrinkling analysis by using the finite element method and the development of analytical solutions in this study. These will be discussed in the following chapters.

2.2 Square Membrane Model

A simple model of a square membrane of a 0.035 mm thick Kapton membrane of edge length 200 mm was cut from the sheet using a square template made of hard cardboard. Two tabs made of Polymide adhesive tape were attached to the four corners. Polymide adhesive tape which has the same properties as Kapton, was used to minimise the stiffening effects of the tabs at the corners of the membrane.

A hook with a thin Kevlar line was attached to each tab, and the lines were hung over pulleys along each side of a frame. This frame consisted of four posts and held by an Aluminium-alloy plate. The pulleys were adjustable in height to align the horizontal level of the membrane. Different fitting could be mounted to the tip of each post to allow various combinations of boundary and loading

[1] For inflated structures

conditions to be applied. Then, small weights were attached to all four cables with the membrane hanging free, only supported by the tension produced by the weights. The details of the experiment set-up are shown in Figure 2.1.

Two loading conditions were applied to the membrane. First, equal masses equivalent to 10 N, were gradually attached to all four cables. Next, masses equivalent to 8 N were attached to one pair of diagonal corners, and small masses equivalent of 1 N were attached to the other pair of diagonal corners. The second loading was intended to produce a much obvious wrinkle pattern in the membrane. The membrane was then unloaded and the transition from the wrinkled to the unwrinkled state of the membrane was observed and compared. The initial condition of the membrane was assumed to be free from any wrinkles before the load was applied.

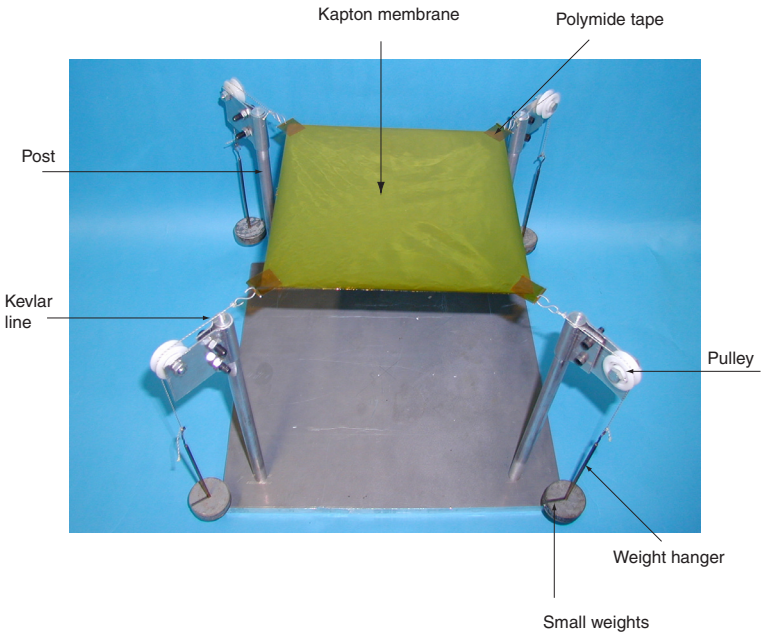

Figure 2.1: Wrinkle observation experiment.

2.2.1 Observations

This experiment was used to simulate a partly wrinkled membrane. In the first load case, when equal masses were attached to the membrane, wrinkles were observed spreading out from the corners and a slightly slack region was developed at the edges. The membrane was then reversed and loaded again to check the slack regions at the edges. The slack edges were observed not to be due to the loading condition. They may be due to manufacturing imperfections of the membrane or introduced during the cutting of the sheet. Due to the constraint

in size of the membrane, the amplitude of the wrinkles was too small to make any measurements possible.

In the second case, a clearly visible half wavelength wrinkle formed at the center of the membrane. The amplitude of the wrinkle reduced towards the edges and corners of the membrane. Wrinkles with two sine waves but small amplitudes were also observed at all the corners. The wrinkle pattern is shown in Figure 2.2. The amplitude of the wrinkle at 8 N ranged from 1.0–1.3 mm, with a maximum wavelength of 22 mm at the center. The measurements were taken with a scaled ruler, by visual inspection.

Several sizes of tab were used to investigate the effects of tab size on the wrinkles formed in the membrane. It was found that the wavelength of the wrinkle was not dependent on the size of the tab used.

At the stage when masses were being added to two diagonal corners of the membrane to grow the wrinkles, we found that the wrinkles formed in the membrane could actually be eliminated by applying a lower load at the two other corners. The amount of load needed to make the wrinkle completely vanish was approximately half of the load applied in the other direction. The amplitude of the wrinkle was found to decrease drastically when the membrane was loaded in the other direction, even with small loads. This suggested that prestressing in one direction to provide a minimum stress in the other direction may be sufficient to avoid wrinkle formation. The alternative is the more conventional option of applying biaxial prestress.

This simple model gave a general feel and insight into this problem. However, further investigation is necessary with a larger scale model which would involve more accurate measurement techniques.

It was observed in both cases that the actual magnitude of the load did not affect

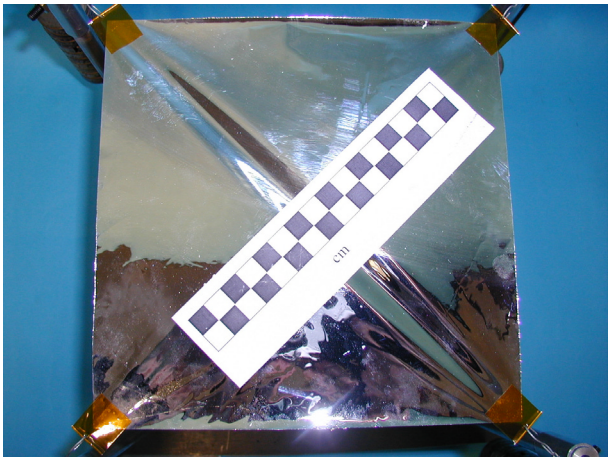

Figure 2.2: Wrinkle observed in the experiment.

the size of the wrinkled region and the wrinkle patterns. The amplitude and wavelength of the wrinkles are the only parameters that change with different loads.

2.3 Membrane Model Subjected to Shear

This model consisted of a wooden "shear frame" connected at the joints with four brass hinges. A rectangular sheet of thin membrane was clamped to the edges of the frame.

The frame was made of four pieces of plywood forming a rectangular frame 400 mm long and 160 mm wide, giving an aspect ratio of 1:2.5. Two 400 mm long wooden blocks and two 160 mm long wooden blocks were connected at right angles with brass hinges to form the bottom frame. This is shown in Figure 2.3, together with a side view showing various components of the model.

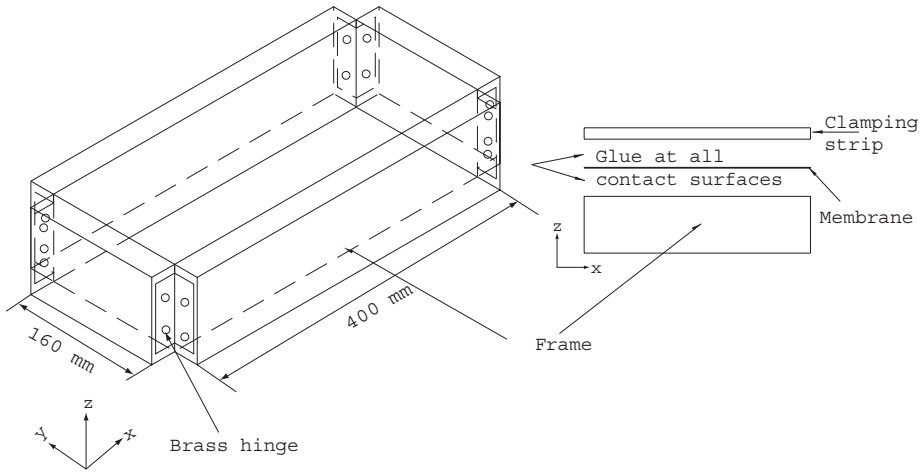

Figure 2.3: Bottom frame and the components of the model.

A rectangular aluminised Mylar membrane of thickness 0.05 mm was cut, lightly prestressed, and pasted on top of the frame. A square grid of 20×20 mm^2 was marked with a permanent ink marker on the membrane over an area of 400×160 mm^2. The grid enabled visual examination of the wavelength and the number of wrinkles in the membrane.

Evo-Stick adhesive was used to glue the membrane onto the bottom frame. The membrane was required to be completely flat at the initial stage before any load application. Therefore, the membrane was laid and small weights were hung at the edges at intervals of 40 mm to give a uniform initial stress to the membrane. The frame was glued to this and the excess membrane was cut and removed.

Four thin wooden strips were glued on top of the membrane edges. A 500 mm square flat steel plate was placed on top of the frame to verify that all the surfaces, i.e. membrane and frames, were intact and clamped. The final model is shown in Figure 2.4.

Figure 2.4: Frame model.

A simple test rig was built to subject the model to pure shear at its upper and lower edges. The test rig was made of 'Dexion 140' steel angles connected with bolts at all its joints. Bracings were provided wherever necessary. It was held in place rigidly with two G-clamps at each side. The frame model was then placed and clamped at its bottom edge in the test rig. A threaded rod was used to displace the frame sideways. This rod was in contact with a target point at the upper edge of the frame, as shown in Figure 2.5.

2.3.1 Observations

Displacements were imposed by adjusting the threaded rod. The displacement was applied in increments of 1 mm, this being measured by using a scale at the top of the test rig. Since Mylar is quite a stiff material, the maximum horizontal displacement of the model was restricted to 8 mm. Here, the shear angle is fairly small.

Wrinkles formed immediately in the membrane, once the upper edge was displaced. When the upper edge achieved 1 mm displacement, the positions of the wrinkled region in the membrane was identified. A line was drawn with red ink marker in the direction perpendicular to the tension lines in the region. The wavelengths of the three most clearly defined wrinkles in the region were measured with a scale ruler and recorded. The procedure was repeated for every 1 mm increment until the 8 mm displacement in the upper edge of the frame was attained.

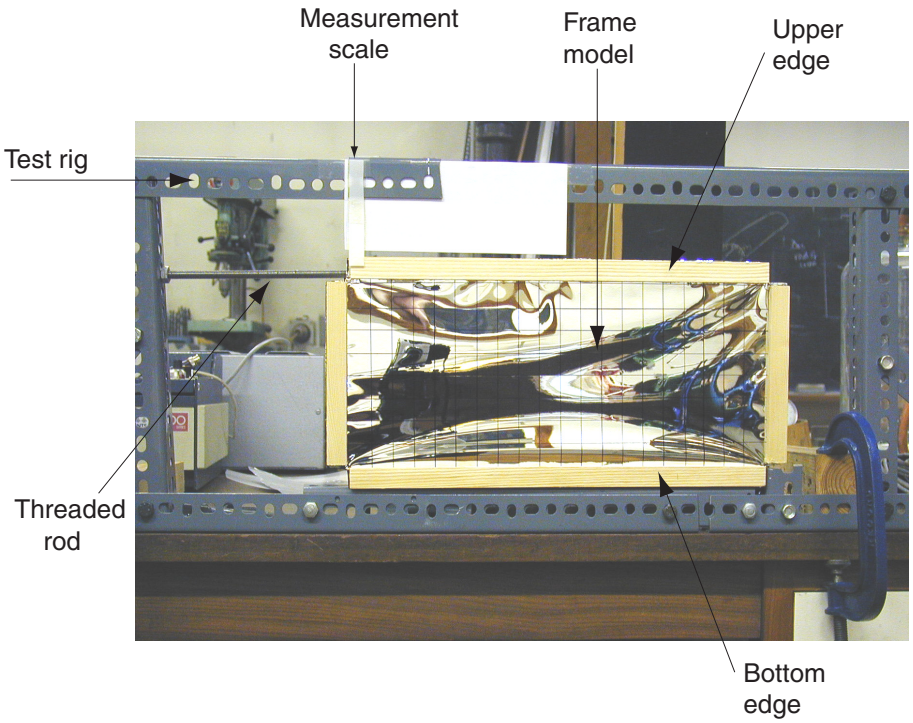

Figure 2.5: Simple test rig for the frame model.

As we increased the displacement, the wavelength of the wrinkles decreased, as shown in Figure 2.6, but the rate of change was found to be declining as the displacement increased. The number of wrinkles found in the membrane initially increased with the load, but after a displacement of 4 mm it became stable. The observed amplitudes of the wrinkles increased with displacement although they were relatively small in magnitude.

We then unloaded the membrane by releasing the displacement. The wavelengths at each 1 mm were again measured and compared to the loading state. After the membrane was fully unloaded, we found that the membrane was a little slack compared to the start of the test. It indicated that some of the initial small tensile stress in the membrane had vanished. This may be due to plastic deformation of the membrane, but more likely this may be attributed to creep. Another possibility may be that the membrane was not rigidly clamped within the frame, i.e. the membrane moved.

The test was then repeated with different materials with different thickness, i.e. a Kapton membrane with thickness of 0.035 mm and another frame—provided by Professor Calladine—with a 1 mm thick rubber membrane. We observed that the wrinkle parameters, i.e. wrinkle wavelength, amplitude and number of wrinkles were dependent on the thickness and the material used. A summary of the observations for the three materials is given in Table 2.1. Also, the final wrinkle patterns for the materials are shown in Figure 2.7. Finally, the average

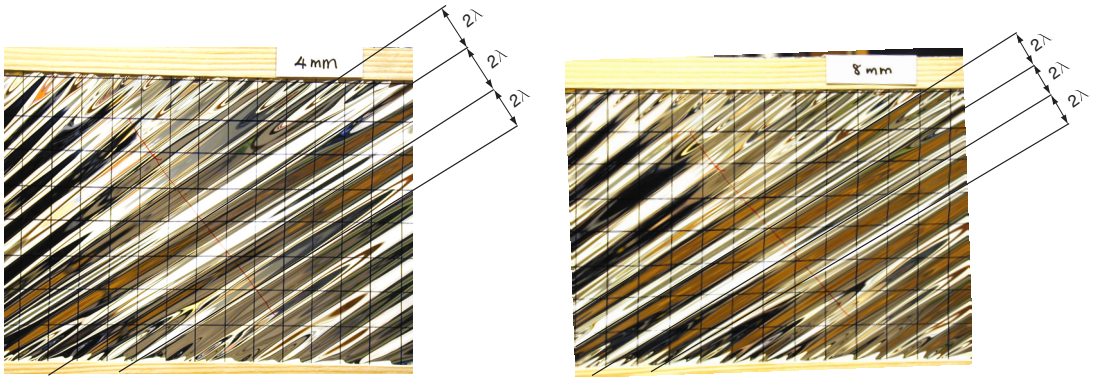

(a) Wavelength at 4 mm displacement.

(b) Wavelength at 8 mm displacement.

Figure 2.6: Wavelengths at 4 mm were larger than at 8 mm.

Material	Thickness (mm)	Amplitude (mm)	Wavelength, 2λ (mm)	Number of wrinkles
Mylar	0.05	3.0	30.5	13
Kapton	0.035	2.5	25.2	21
Rubber	1	7.0	71.0	3

Table 2.1: Summary of observations for different materials at 8 mm displacement.

wavelength for each material was plotted against the displacement and is shown in Figure 2.8.

Figure 2.8 shows that the relationship between the wavelength and the displacement is a hyperbolic function. In conclusion, the observations from the experiments have shown that

$$2\lambda \propto \frac{1}{\triangle^i} \tag{2.1}$$

where λ is the half wavelength of the wrinkle, $\triangle$ is the displacement and i is the hyperbolic relationship between wavelength and the displacement.

The simple experiments discussed in this chapter were intended as initial observations, hence the data collected was not particularly accurate. However the observations and results obtained have given a good prediction of the wrinkle patterns and the behaviour of the wrinkled membrane. Therefore, these results will be used as a basis for the numerical and analytical analysis which we will discuss in the following chapters.

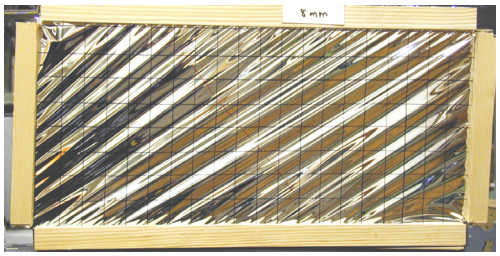

(a) Mylar membrane.

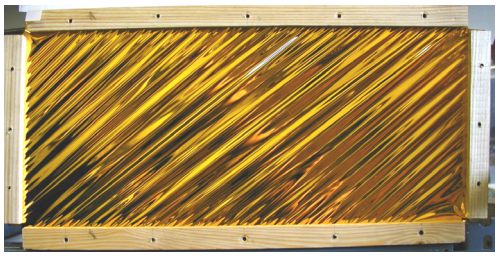

(b) Kapton membrane.

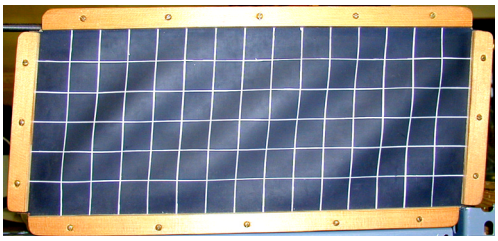

(c) Rubber membrane.

Figure 2.7: Final wrinkle patterns for different materials, at 8mm displacement.

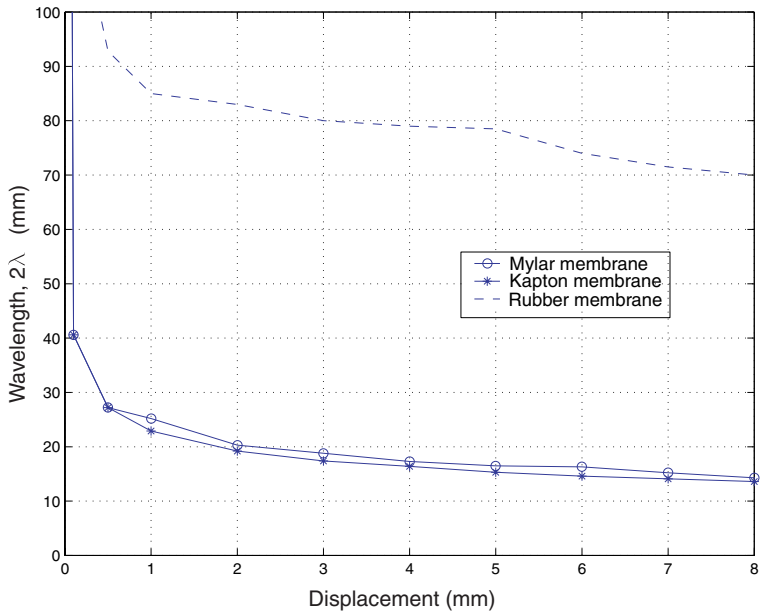

Figure 2.8: Plots of wavelength against displacement for different materials.

Chapter 3

Finite Element Analysis— No-compression Material Model

There is no standard way of implementing a wrinkling condition in ABAQUS (1998). Hence, wrinkling was simulated by using different standard elements available in the package, incorporating the no-compression elasticity behaviour in the material definition, and then performing a geometrically non-linear analysis.

3.1 Element type

Two standard elements available in ABAQUS were chosen, namely membrane and shell elements. The general description and characteristics of these two elements are given below.

The main characteristic of membrane elements is that they are true 2-D elements in which bending stiffness is neglected. They model in-plane translations with two Degrees of Freedom (DOF) and have no out-of-plane stiffness. Therefore, an analysis which requires out-of-plane translations must first be analysed statically in-plane to apply tension to the structure. However, compressive stresses can arise which produce negative geometric stiffness terms for these elements. When this situation occurs, numerical singularity problems are encountered in the next step when performing an out-of-plane non-linear analysis.

Shell elements have five or six DOF at each node, three translations and two or three out-of-plane rotations, depending on the element formulation. This means that a buckling analysis can be performed successfully if a membrane is modelled as a shell structure. However, to properly resolve the wrinkles, a very fine mesh—smaller than half the wavelength of the wrinkle—is required[1]. A further problem with thin shell models is that singularities and/or pivoting problems can occur,

[1] cf.Nyguist frequency in signal analysis (Ewins, 1995).

depending upon the model.

3.1.1 Geometric Non-linearity

To avoid compressive stresses, a membrane tends to deform out-of-plane: this results in the formation of wrinkles. The out-of-plane deformation may involve large translations and rotations hence the behaviour of the membrane is clearly geometrically non-linear.

Large displacement effects on the membrane can be simulated by including the NLGEOM parameter in the *STEP option in ABAQUS. Thus, all the elements are formulated in the current configuration and so the elements distort from their original configuration as the deformation increases.

The stress calculated by incorporating this parameter is the Cauchy ("true") stress. The stress components for a membrane element are given in the global directions, while for shell elements they are given in the local directions that rotate with the elements.

3.1.2 No-compression Material

It is assumed that a membrane is incapable of carrying compressive stress. Wrinkles form immediately when a compressive stress is about to be applied within the membrane. This behaviour can be simulated with the no-compression elasticity option in ABAQUS.

This option modifies the elastic behaviour of the model by firstly solving for the principal stresses assuming linear elasticity. Then, any compressive principal stresses are set to zero and the associated stiffness matrix coefficients are also set to zero. The directions in which the principal stresses are set to zero are recalculated at every iteration, hence the results are not history dependent. This analysis was carried out based on the Stein-Hedgepeth's wrinkling theory and the principal stress wrinkling criterion stated in Section 1.3.5 was used.

Convergence difficulties were encountered when the no-compression option was first used. This was mainly due to problems with zero pivots, i.e. a force has been applied to a degree of freedom that had no stiffness. As explained above, this can happen when stiffness matrix coefficients corresponding to the compressive principal stresses are set to zero, hence the model can become unstable.

Two different techniques were used to stabilise the model with no-compression behaviour. They are explained next.

3.1.3 Artificial Stiffness

The singularities that occur due to the loss of stiffness in compression material can be overcome by overlaying the no-compression membrane element with another element that has a small Young's modulus relative to the membrane element.

In this analysis, a thin triangular facet shell element (STRI3) with a Young's modulus of 1% the value of the membrane element's Young's modulus was used. The STRI3 element is a plate element used to approximate a shell, it has three nodes, each with six degrees of freedom. All membrane elements were overlaid directly with shell elements in their original configuration, to create a small artificial stiffness, which then stabilised the membrane model.

3.1.4 Strain Energy Stabilisation

Wrinkling is a localised instability, hence the commonly used methods for stability and postbuckling analysis which for the treatment of global instability, e.g. the arc length method, are not suitable. But ABAQUS provides an automatic mechanism which applies volume proportional damping to the structure to dissipate the local transfer of strain energy from one part of the model to neighbouring parts.

This mechanism can be invoked by including the STABILIZE parameter in a non-linear static analysis. The analysis assumes that the problem is stable at the beginning of the step, but an instability may develop in the course of the step. When an instability is detected, ABAQUS adds viscous force

$$F_v = c\dot{u}$$

to the global equilibrium equations

$$m\ddot{u} + c\dot{u} + ku = 0$$

where m is the artificial mass calculated by ABAQUS assuming unit density of the structure, c is a fictitious damping coefficient, $\dot{u} = \triangle u/\triangle t$ is the vector of nodal velocities, $\ddot{u} = \triangle^2 u/\triangle t^2$and $\triangle t$ is the time increment.

If a local region goes unstable, i.e. wrinkling occurs, the local velocities increase and as a result, damping is applied to dissipate part of the strain energy released. The damping coefficient, c, is automatically calculated by ABAQUS based on the solution at the first increment of the step.

3.2 Square Membrane Analysis

A square membrane structure similar to the simple experiment discussed in Chapter 2 was analysed to test the algorithm for wrinkling analysis stated above. A full model of 200×200 mm^2 was used in the analysis. The model was supported by the symmetrical loading applied at the corners of the membrane, hence no constraints at the boundaries were applied to simulate the experiment.

We used 722 3-node linear membrane elements (M3D3) and 722 3-node facet thin shell elements (STRI3) in the analysis. The following material properties for the Kapton membrane were used: Young's modulus, $E = 3740$ MPa; Poisson's ratio, $\nu = 0.35$; and the sheet thickness, $t = 0.035$ mm. Elements with different thickness, i.e. $t = 0.16$ mm were used at the corners to simulate the effects of the Polymide tape.

The wrinkling analysis was performed to simulate the second load case in the experiment described in Section 2.2. The model was subjected to a higher in-plane load of 8 N applied at one pair of diagonal corners, and a lower load of 1 N at the other pair of corners. The FE model is shown in Figure 3.1.

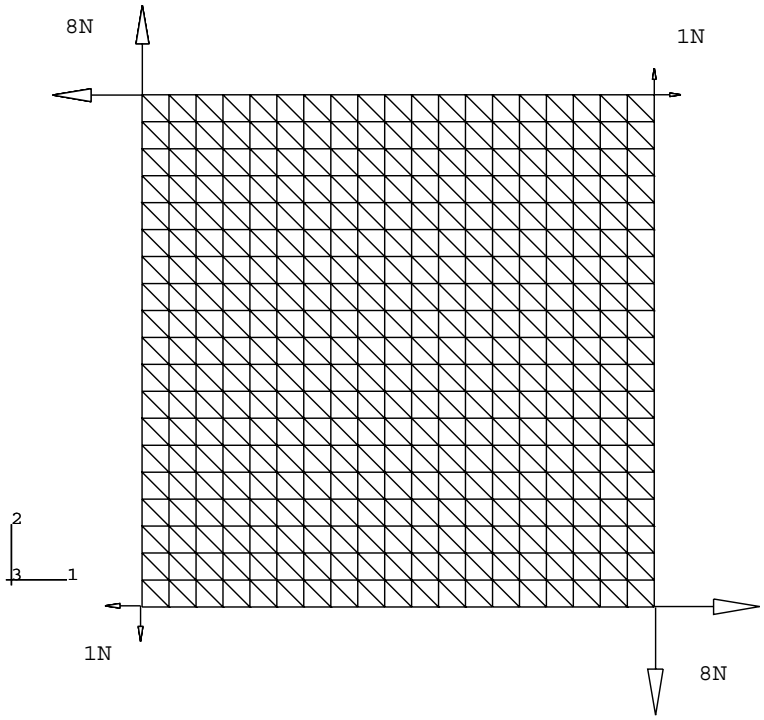

Figure 3.1: FE model of square membrane.

An analysis was carried out with the two different stabilisation methods outlined in the previous sections. Comparisons were made between the convergence rate of the different methods. The convergence rate was very slow with both methods.

The model became very unstable as the load increased and there were many numerical singularities in the analysis and divergence occurred.

The default convergence control parameters in the ABAQUS non-linear analysis were adjusted to improve the solution efficiency. After modification of the control parameter, a wrinkling analysis was successfully implemented involving geometric non-linearity, no-compression material and artificial stiffness. The stress state in the membrane, i.e. the magnitude and directions of the principal stresses at the wrinkled region were obtained and are shown in Figure 3.2. ABAQUS has plotted the principal stresses at each node as a vector with length proportional to the stress; the direction of this vector corresponds to the principal stress direction.

Note that the major principal stresses in Figure 3.2(a) are tensile and the stress distribution at the center of the membrane is fairly uniform. A much higher stress occurs at the corners. As for the minor principal stress plot in Figure 3.2(b), we observe positive stress in the taut regions. In the wrinkled region all minor principal stresses are zero. Since wrinkles form along the direction of tensile stresses, the wrinkle pattern in the model is determined in Figure 3.2. This showed that the wrinkles formed at the center of the membrane along the higher loaded diagonal, and also that they formed at all the corners. Slack regions are found at the edges when both principal stresses are zero. The wrinkle patterns in the analysis were similar to those observed in the experiment as shown in Figure 2.2.

Since only in-plane translations are defined for a membrane element, the results shown in Figure 3.2 are purely two-dimensional. To determine the out-of-plane deformation of the membrane, i.e. the amplitude of the wrinkle in the wrinkled region, a simple analytical wrinkle model has been developed. A program was written implementing this model to predict and determine the amplitude of the wrinkle. The algorithm of the program and the simple analytical wrinkle model are discussed next.

3.3 Wrinkling Program

A program was written in Matlab (1993) as a post processer to determine the wrinkling pattern of a membrane that has been previously analysed in two dimensions with ABAQUS. The main objective of this program is to determine an upper bound to the magnitude of the out-of-plane deformation, i.e. the amplitude of the wrinkle wavelength that is not obtainable from the finite element analysis using the membrane model. Indeed, the nodal translations and principal stresses obtained are then used in the wrinkling program. The wrinkling program is split into several modules outlined below.

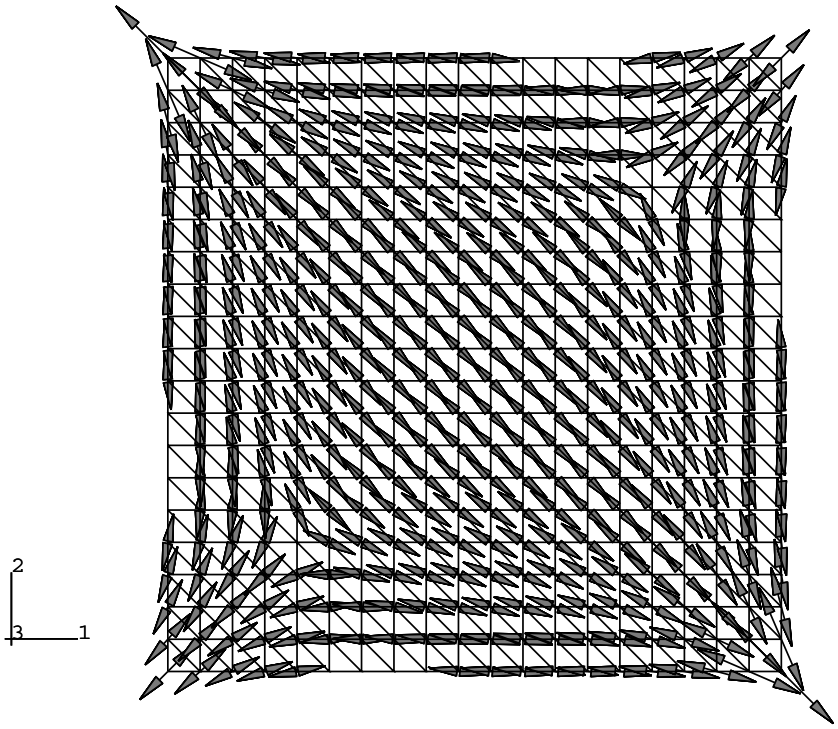

(a) Major principal stress.

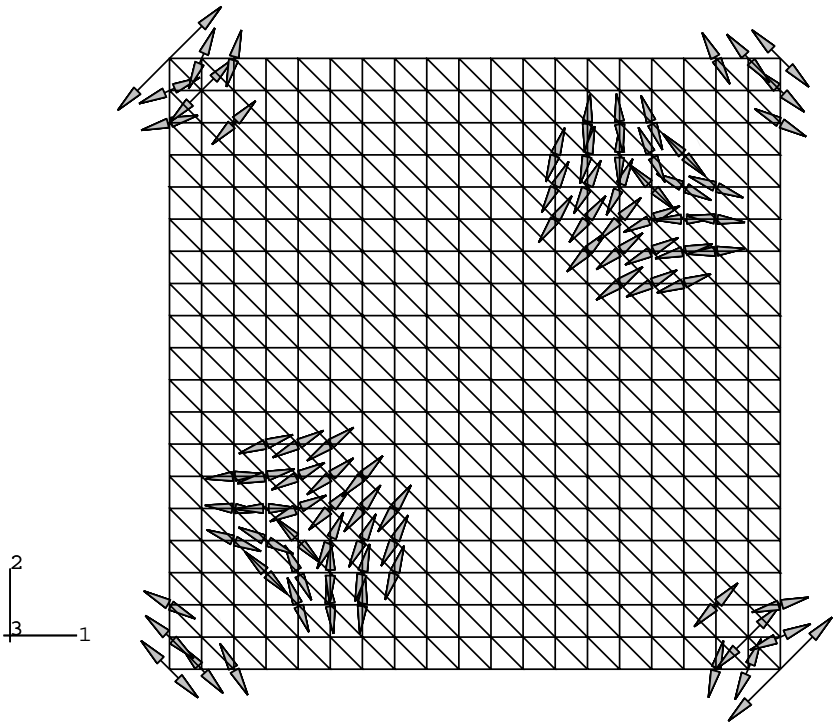

(b) Minor principal stress.

Figure 3.2: Wrinkling analysis using no-compression material.

3.3.1 Algorithm

Wrinkles are formed in the direction of the major principal stress and are thus perpendicular to the direction of the minor principal stress. Vector plots of the principal stresses can be used to determine the wrinkled regions in the membrane. Figure 3.3(a) is a plot, produced by the Matlab program, showing the direction and magnitude of the positive principal stresses at points where the minor principal stress is zero.

The program displays a vector plot of the principal stress and the user defines the wrinkled regions by "clicking" in the Matlab figure window on the elements that define the boundary of each wrinkled region. It is intended to enhance this facility in future to become fully automatic, but the user input facility gives greater flexibility. An advantage of this flexibility is that the user decides if neighbouring wrinkled regions should be joined together or not. Also, the effects of different types of wrinkle boundaries toward the wrinkle parameters can be investigated by defining different wrinkle boundaries, e.g. an elliptical wrinkle boundary or a more general rectangular boundary. The user-defined wrinkled boundary for the problem in Section 3.2 is shown in Figure 3.3(b).

After defining the boundary of each wrinkle, the program reads the in-plane nodal displacements of the nodes along this boundary from the finite element analysis and gives a simple prediction of the out-of-plane deformation of the membrane. The out-of-plane deformation of the membrane is determined by the simple wrinkle model illustrated below.

3.3.2 Simple Wrinkle Model

For simplicity, we assume that there is only one predominant[2] wrinkle in the wrinkled region and the shape of this wrinkle is assumed to be parabolic. This also assumed that the unwrinkled regions remain perfectly flat.

Hence, if we consider a cross-section through the wrinkle in Figure 3.3(b), the out-of-plane deformation is at a maximum at the center of a parabola, gradually reducing to zero at the two ends as shown in Figure 3.4.

Consider two points lying on either side of a wrinkle, Q and P. In the displaced configuration, they move to $Q^{'}$ and $P^{'}$, respectively. The initial distance between Q and P is L and the final length is L'. From the finite element analysis the displacements of Q and P in the direction QP can be determined. Let these be δQ and δP, and calculated as follows:

[2]If there is more than one wavelength, the amplitude of the assumed predominant wrinkle is the sum of all the amplitudes in the wavelength.

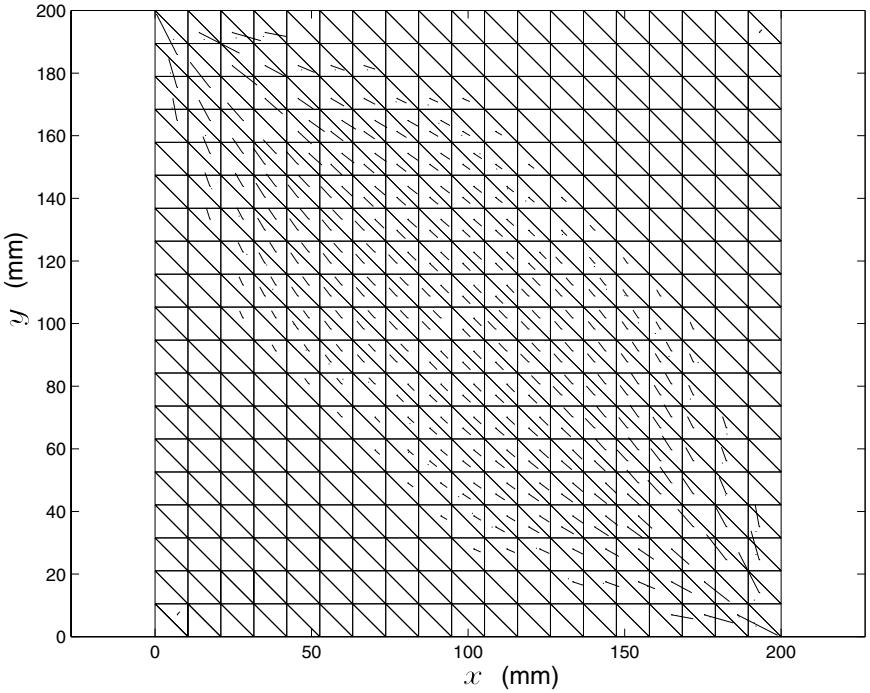

(a) Major principal stress in wrinkled region.

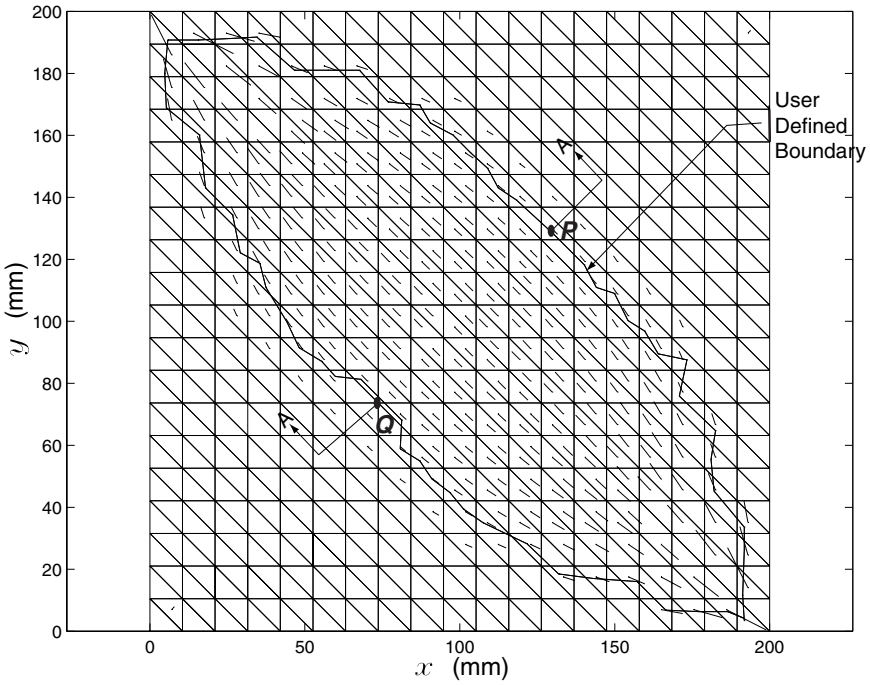

(b) User defined wrinkled boundary.

Figure 3.3: Wrinkle pattern from wrinkling program.

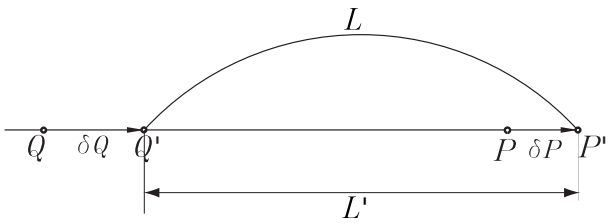

Figure 3.4: Simple parabola wrinkle model, section A-A of Figure 3.3(b)

$$L = \sqrt{(x_P - x_Q)^2 + (y_P - y_Q)^2} \tag{3.1}$$

$$\delta Q = Q^{'} - Q = \sqrt{(x_{Q'} - x_Q)^2 + (y_{Q'} - y_Q)^2} \tag{3.2}$$

$$\delta P = P^{'} - P = \sqrt{(x_{P'} - x_P)^2 + (y_{P'} - y_P)^2} \tag{3.3}$$

$$L^{'} = L - \delta P \pm \delta Q \tag{3.4}$$

where x and y are the in-plane coordinates of the membrane. The sign in Equation (3.4) depends on the direction of the displacement at the end Q' of the wrinkle. If the final length L' is shorter than the initial length, L, i.e. $L' < L$, then a wrinkle is formed in the membrane.

Amplitude of Wrinkle

Since a wrinkle of parabolic shape was assumed, the amplitude of the wrinkle can be determined by considering the equation of a parabola, see Figure 3.5.

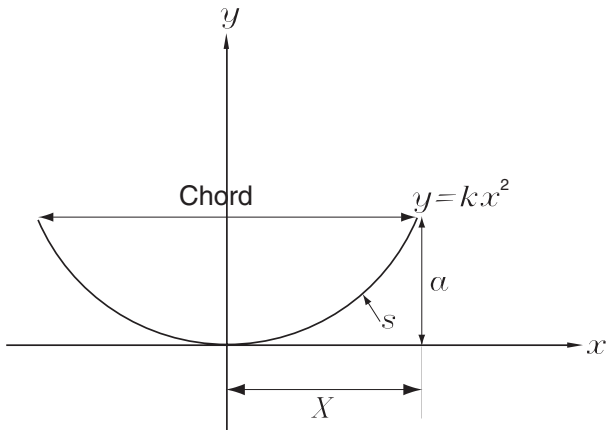

Figure 3.5: Parabola

$$y = kx^2 \tag{3.5}$$

$$\frac{\mathrm{d}y}{\mathrm{d}x} = 2kx \tag{3.6}$$

To determine the amplitude, the coefficient k in Equation (3.5) has to be determined. Assigning the arc length of the curve, s = initial length = L in Equation (3.1), and the chord = final length = $L' = 2X$ in Equation (3.4)

$$\begin{aligned} s &= 2\int_0^X \sqrt{\mathrm{d}x^2 + \mathrm{d}y^2} \qquad (3.7)\\ &= 2\int_0^X \sqrt{1 + \left(\frac{\mathrm{d}y}{\mathrm{d}x}\right)^2}\\ &= 2\left[x + \frac{4k^2}{2}\frac{x^3}{3}\right]_0^X\\ &= 2X + \frac{4}{3}k^2X^3 \qquad (3.8) \end{aligned}$$

Substitute $X = L'/2$

$$k = \sqrt{(s - L')\frac{3}{4}\left(\frac{2}{L'}\right)^3} \tag{3.9}$$

The analysis becomes more complicated when wrinkles occur at the free edges of the membrane. In this case, we assume that the maximum amplitude of the wrinkle occurs at the edge. Therefore, Equation (3.9) is modified by assuming $X{=}L'$, then

$$k = \sqrt{\left(\frac{s}{2} - L'\right)\frac{3}{2}\left(\frac{1}{L'}\right)^3} \tag{3.10}$$

Note that the particular loading condition of the square membrane gives high tension at the center of the membrane, thus the complication of the free edges is avoided. Then, the amplitude, a, of a wrinkle can be determined from

$$a = kx^2 \tag{3.11}$$

In the calculation of the amplitude of the wrinkles, the edge displacements are taken from the x and y coordinates of the boundary of the wrinkled regions defined by the user. Instead of considering actual direction of the wrinkle and taking the cross-section, we first calculate the amplitude in x–z plane, and then repeat in y–z plane. The amplitudes of the wrinkle are the average of these values. The plot of the out-of-plane deformation of the square membrane from the wrinkling analysis is shown in Figure 3.6 with a maximum amplitude of 1.4 mm. This gave a very close approximation to the experimental observations where a maximum amplitude of 1.3 mm was measured. Therefore, the wrinkling analysis using the procedures described in Section 3.1 was verified.

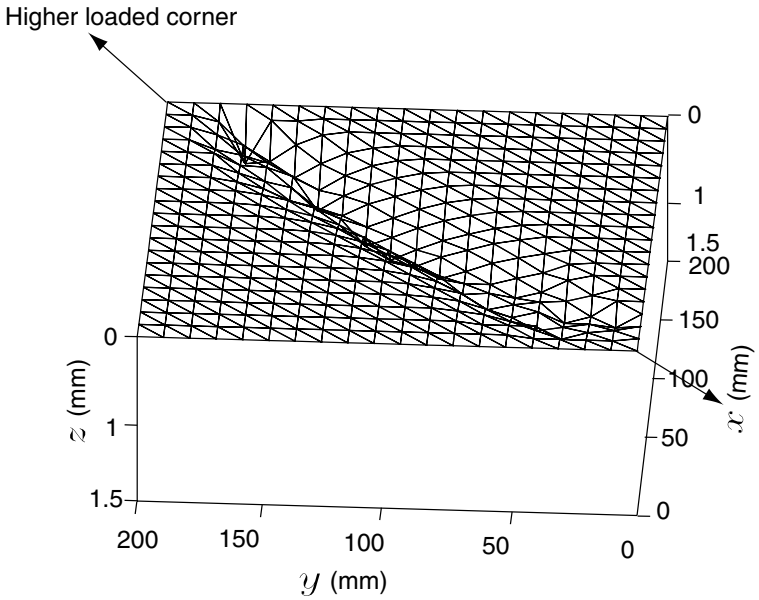

Figure 3.6: Out of plane deformation using simple wrinkle model.

3.4 Inflated Party Balloon

The second model that has been analysed is a circular party balloon made of aluminised Mylar with a diameter of 460 mm (uninflated) and subjected to a uniform pressure of 0.0042 MPa. The following material properties were used: Young's modulus, $E = 588$ MPa, Poisson's ratio, $\nu = 0.35$, and sheet thickness, $t = 0.05$ mm.

Prior to performing the full wrinkling analysis, several FE models using 3-node linear membrane elements (M3D3) and 4-node linear membrane elements (M3D4) were investigated. We found that all models predicted the same number of folds (a fold is a very deep wrinkle in which there is contact between the material on the two sides of the wrinkle) but their actual position was mesh dependent, since they developed at mesh interfaces. The final FE model shown in Figure 3.7, comprised both M3D3 and M3D4 in a random mesh. The membrane elements were overlaid with 3-node facet thin shell elements (STRI3). By applying appropriate boundary conditions and symmetry, only the upper half of the balloon had to be modelled.

The wrinkling analysis procedures used in Section 3.2 were applied to this model. Initially, the balloon was in a flat circular configuration. A uniform pressure distribution was applied to the inner surface. Since the pressure loading was acting normal to a surface that had no bending stiffness, numerical singularities occurred. Therefore a small uniform tensile stress was applied to all the membrane elements as an initial condition prior to the first step of the analysis, and the edges of the membrane were subjected to in-plane constraint. A small initial load step

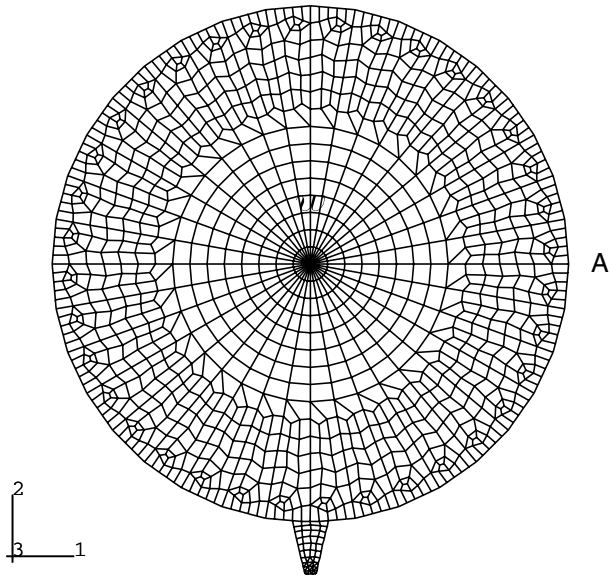

Figure 3.7: FE model for party balloon.

Model	Experiment	FEM
Center Deflection, w (mm)	106.0	115.4
Edge displacement, u_A (mm)	52.0	50.2
Depth of wrinkle (mm)	2–9.1	3.1–8.8
Number of wrinkles	17	19

Table 3.1: Comparisons between the physical and FE model.

was also needed to achieve a smooth initial curvature of the balloon. The initial stress and the edge supports were removed after the first load step to eliminate any effects on the final solution.

A physical model was tested and several parameters were recorded to compare with the results obtained from the FE model (see Figure 3.8). The comparisons of the vertical displacement at the center, w, of the balloon, the horizontal displacement of edge point A, u_A, the depth of the wrinkle[3] and the number of wrinkles[3], are given in Table 3.1.

3.4.1 Discussion

The results showed that the FE model simulates the deformed configuration of the balloon reasonably well. It gave close results for both the displacement of the apex, and the lateral displacement at point A of the inflated balloon. The

[3]These measurements were obtained by scaling from the plot in Figure 3.8.

Figure 3.8: Comparison between FE model and physical model.

number of wrinkles predicted was slightly higher than in the physical model.

The FE model was only capable of simulating the size of wrinkles ranging from 3.1 to 8.8 mm; this predicted 15 big folds and 4 smaller ones. There were 14 big folds and 3 smaller wrinkles in the physical model. However, the finer wrinkles with very small amplitude between the big folds and at the transition region between the taut and mid-plane observed in the physical model were not successfully predicted.

As can be seen in Figure 3.9, a contour plot of major principal stress in the balloon shows that a very uniform distribution of stresses was obtained at the top of the balloon, represented by zones 1, and 2. Wrinkles started forming in zones 3 and 4 and at the equator of the balloon. This result agreed with the study conducted by Greschik et al. (2000) on a inflated membrane reflector. The position of the wrinkles in the FE model was mesh dependent, hence a refinement of the mesh in the wrinkled region may be required to simulate the finer wrinkles.

Generally, the wrinkling analysis has successfully predicted the overall wrinkle pattern in the balloon in its inflated state and the number of big folds along the balloon's equator.

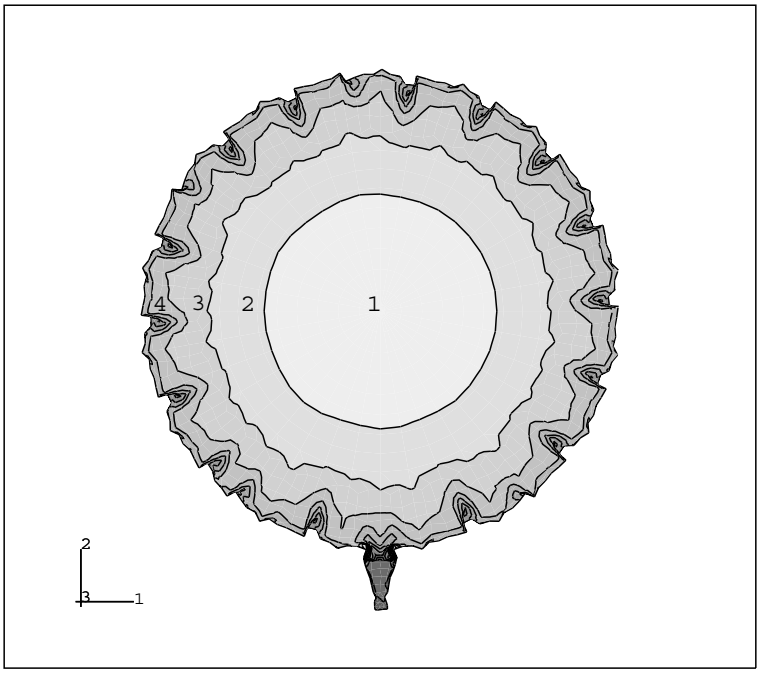

Figure 3.9: Contour plot of major principal stress in the inflated balloon.

Chapter 4

Finite Element Analysis— Non-linear Shell Model

A distinguishing characteristic of membranes is that they are sufficiently thin to neglect their bending stiffness. This assumption has been used in the analysis of wrinkling by the tension field theory and the Stein-Hedgepeth theory. If this assumption is incorporated into a FE code, the results presented in Chapter 3 are obtained.

However, wrinkles form when a compressive stress is applied to the membrane. This situation is similar to the buckling of a plate with very small bending stiffness. Using the critical compressive stress theory suggested by Rimrott and Cverco (1985), it seems appropriate to treat wrinkling by employing bifurcation buckling theory. In the following sections, buckling modes are predicted using an eigenvalues analysis of the tangent stiffness matrix. Subsequently, geometrical imperfections are introduced into the initially flat surface and then analysed using a geometrically non-linear finite element procedure in ABAQUS. This analysis procedure is then tested with one of the classical problems that were solved by Mansfield (1968).

4.1 Prediction of Failure Modes

In ABAQUS, an eigenvalue buckling prediction can be performed by including the *BUCKLE parameter in the *STEP option of the analysis. In this procedure, we are looking for the bifurcation/buckling loads for which the tangent stiffness matrix become singular. When this situation happens, the solution is solved as an eigenvalue problem.

The problem may be written as:

$$(\mathbf{K}_0 + \lambda_i \mathbf{K}_\triangle)\mathbf{v}_i = 0 \tag{4.1}$$

where $\mathbf{K}_0$ is the stiffness matrix corresponding to the initial state, including any initial effects of the preloads, $\mathbf{K}_\triangle$ is the differential initial stress and load stiffness matrix due to the incremental loading pattern; λ_i and $\mathbf{v}_i$ are the eigenvalues and eigenvectors/mode shapes, respectively.

Generally the lowest value of λ_i is of most interest and the buckling mode shape, $\mathbf{v}_i$, is normalised so that the maximum displacement component has unit magnitude. These vectors are the most useful outcome of this analysis since they provide an initial prediction of the failure mode of the structure by buckling. Introduction of appropriate geometric imperfections into the model allows us to proceed with the wrinkling analysis.

4.1.1 Introduction of Geometric Imperfections

The model becomes unstable when the bifurcation point is reached; this situation occurs when the model is about to wrinkle/buckle. The equilibrium path should then be switched to an alternative, lower stiffness path. The eigenvectors obtained in the eigenvalue buckling analysis give the possible failure modes. To force the structure to change path, we introduce geometric imperfections into the initial "perfect" geometry, based on a linear superposition of buckling modes, using the corresponding displacements obtained from the analysis (Allen and Bulson, 1980).

The introduction of imperfections in the geometry of a structure tends to turn the equilibrium path into a continuous response where the buckling mode becomes more dominant as the critical load is approached. This can be activated in ABAQUS by using the *IMPERFECTION option in the form of:

$$\triangle x_i = \Sigma_i^M w_i \phi_i \tag{4.2}$$

where w_i is the i^{th} mode shape and ϕ_i is the associated scale factor.

The lowest buckling modes are assumed to provide the critical imperfections hence the largest factor should be used for the lowest mode. The magnitude of the perturbation is typically from 5 to 50% (ABAQUS, 1994) of the relative structural dimension, i.e. shell thickness. It is important to determine the structural response to the imperfection in the original geometry by conducting several analyses to investigate the sensitivity of the structure to imperfections.

4.2 Rectangular Membrane Model

The rectangular membrane clamped at all the edges and subjected to shear displacement (see Section 2.3) was modelled and analysed by using the procedures listed above. The membrane had dimensions of 400×160 mm^2.

We used the four-node S4R5 thin shell element, reduced integration with hourglass control and five DOF to model the membrane: i.e. three in-plane translations and two in-surface rotation components per node. The following material properties for the Mylar membrane were assigned: Young's modulus, $E = 6460$ MPa; Poisson's ratio, $\nu = 0.35$; and sheet thickness, $t = 0.05$ mm. Two-node frame elements, (FRAMED2D) were employed at the edges of the membrane to model the timber frame. Multi-point constraints (MPC) were used to connect the shell elements and the frame elements at all the edges.

The model was restrained in its out-of-plane DOF at all edges, and all DOF at the bottom edge were suppressed to simulate the frame being clamped rigidly in the experiment. Then, the upper edge was given a total displacement of 8 mm in the horizontal direction.

4.2.1 Analysis

Since the membrane is very thin, the model may be sensitive to geometrical effects from the pre-load initial state. Therefore, a base state of the membrane was created by applying a small initial stress through a static non-linear geometrical analysis. The top edge was displaced just before the first negative stiffness was found in the system matrix, i.e. below the critical buckling load. This initial small stress was used to stabilise the very thin shell.

Then, the eigenvalue buckling analysis was carried out with a perturbation load in the form of an applied horizontal displacement. Since the lowest eigenmodes were of interest, only the first two eigenvalues were extracted and included in the next analysis step in the form of an imperfection.

In this state, all possible failure modes of the membrane needed to be verified. It was also necessary to ensure that the mesh had been discretised correctly for each mode. From Equation (4.2), the imperfection is the sum of each eigenmode with its associated scale factor, ϕ. This factor is to be assigned by the user according to the eigenmode shapes obtained and compared to the failure modes that are likely to be experienced by the structures.

The first two modes obtained in our analysis are shown in Figure 4.1. A parallelogram wrinkle pattern or buckling mode is expected for a membrane subjected to pure shear and this was agreed with the mode shapes obtained. Therefore, $\phi_1 = 0.5$ and $\phi_2 = 0.5$ were defined to superpose the two eigenmodes.

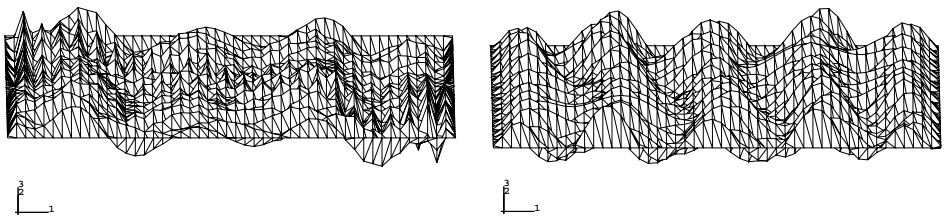

(a) (b)

Figure 4.1: First two eigenmodes predicted by buckling analysis, (a) first mode shape and (b) second mode shape

Then, imperfections were introduced to the initial geometry by combining the two mode shapes with the associated scale factors and multiplied by 10% of the shell thickness. These imperfections involved only the out-of-plane displacements of the mode shapes. The next step of the analysis was to include the static analysis of the membrane subjected to a shear displacement of 8 mm at its upper edge. A full non-linear geometrical analysis was employed for that purpose.

The analysis was successfully implemented with the final wrinkle pattern and its associated wrinkle amplitudes being obtained. Several issues were considered in the analysis to obtain more accurate predictions, including the effects of mesh density and imperfection sensitivity of the model. These are discussed in the following.

4.3 Discussion

4.3.1 Meshing

To model the wrinkles more effectively, different meshes for the same model were tried. We started with a relatively coarse mesh with 3960 4-node thin shell elements and with 19800 DOF. Then, a finer mesh with 15920 elements with 81000 DOF was used and this was followed with the finest mesh of 63840 elements and 320005 DOF. The final FE model mesh used is shown in Figure 4.2. A summary of the results using the three different mesh densities is presented in Table 4.1.

The wrinkles are best seen on a contour plot of the out-of-plane displacements. Each wrinkle was considered to extend from one peak to another peak of the contour, see Figure 4.3. Based on these results and the observations in the experiment (there were 13 wrinkles with maximum amplitudes of approximately 3 mm observed in the experiment), we concluded that the model of intermediate density (15920 elements) best represented the wrinkling condition in this loading

Element	DOF	Inc[a]	Displac-ement (mm)	Number of wrinkles	Amplitude (mm)	Max Principal Stress $(N/mm)^2$
3960	19800	228	8.0	8	3.40	90
15920	81000	271	8.0	10	2.76	97
63840	320005	435[b]	3.3	7	1.62	34

Table 4.1: Comparisons between three different mesh densities for the FE model.

[a]Number of increments required to complete the analysis.
[b]The analysis terminated at this increment due to convergence problems.

condition. The wrinkle patterns from the analysis were similar to the observed wrinkle patterns, see Figures 4.5 and 2.7(a) Therefore, this was the model used to calculate the results presented in this section.

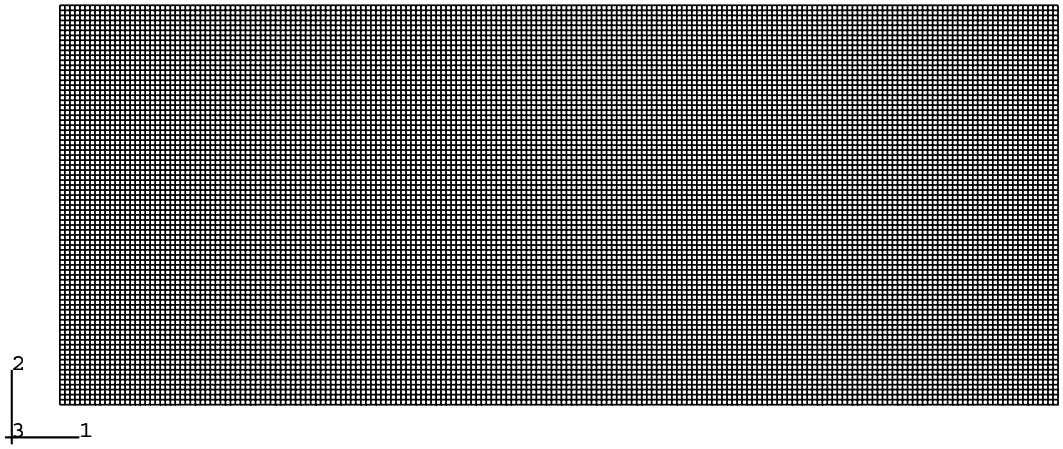

Figure 4.2: Finite Element Model.

The actual location of the wrinkles and the wavelength were found to depend on the mesh density in the finite element analysis. The wavelengths of four wrinkles were measured after every 50 load step increments. We observed that the variation in wavelength against load increments did not follow the same decrease with increase in load that had been observed in the experiments, see Figure 4.7. The reason may be that the density of the mesh used was insufficient to capture small variations in wavelength. Hence, to determine the change in wavelength a finer mesh is proposed.

As shown in Table 4.1, the model with a very fine mesh experienced premature termination of the analysis due to divergence at a certain load step, even though the strain energy stabilisation technique had been activated in the analysis. Continuous remeshing of the wrinkled region and reanalysis with different shell elements may be necessary to model the wrinkles more accurately.

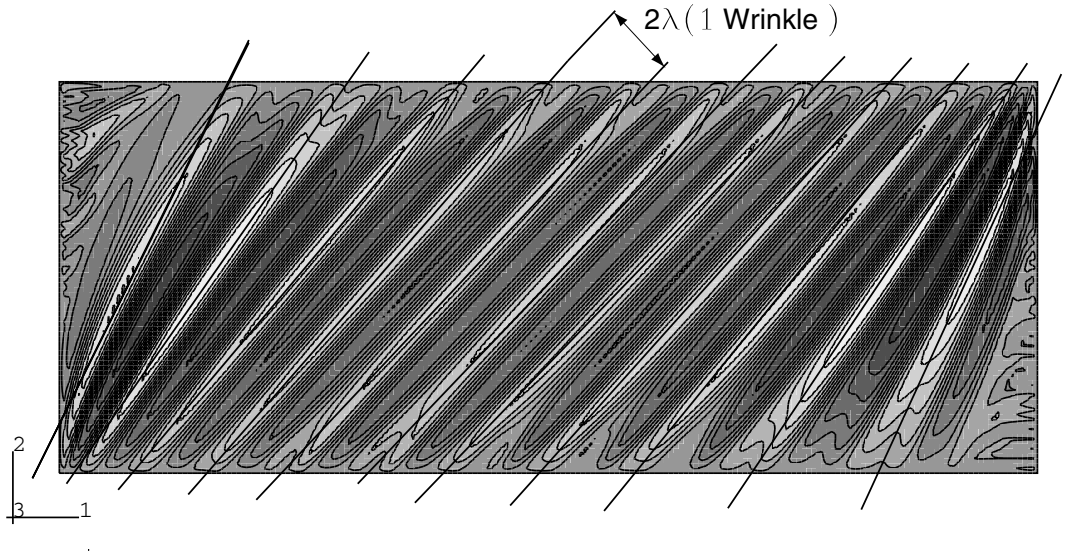

Figure 4.3: Definition of wrinkles from contour plot of out-of-plane deformation.

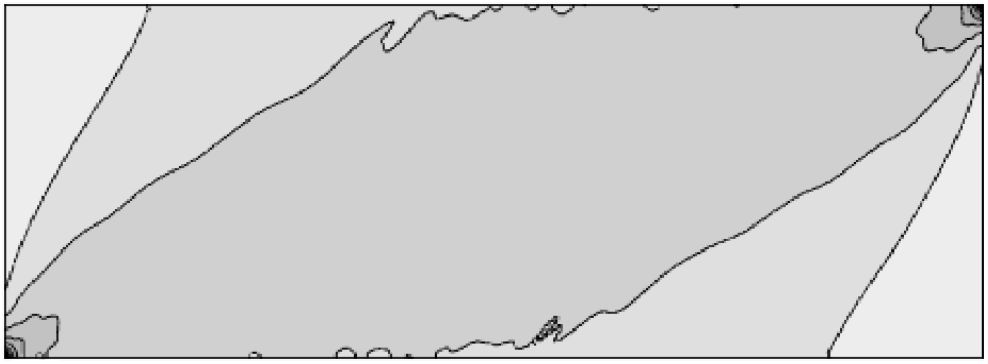

Figure 4.4: Contour plot of major principal stress.

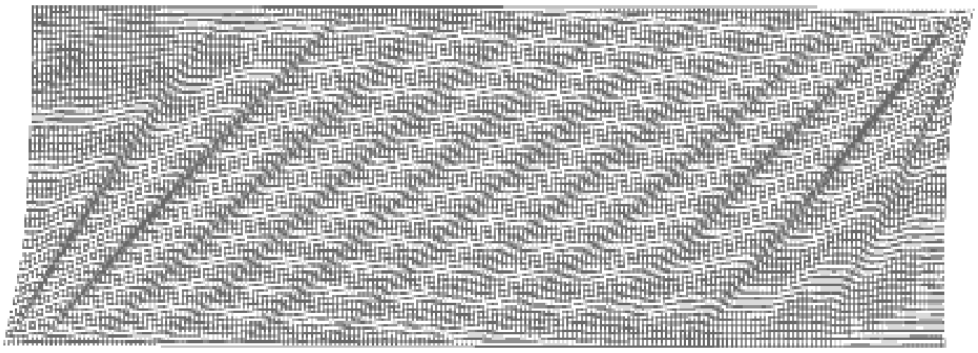

Figure 4.5: Final wrinkle pattern.

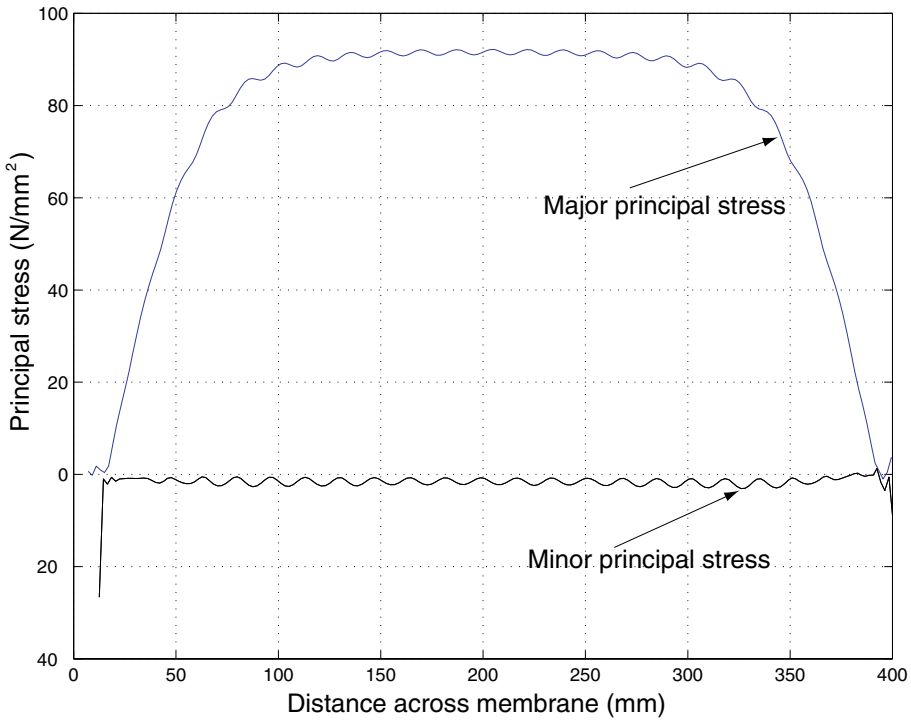

Figure 4.6: Principal stresses variation at mid-plane of the membrane.

IMP[a], %	Mode 1	Mode 2	Mode 1+2 $(0.5 \times 0.5)^b$	Mode 1+2 $(0.7 \times 0.3)^b$	Mode 1+2 $(0.3 \times 0.7)^b$
0.1	2.41	2.33	2.40	2.39	2.33
1	2.47	2.39	2.46	2.45	2.40
10	2.51	2.41	2.50	2.50	2.43

Table 4.2: Comparisons between different magnitude of imperfections with respect to the maximum amplitude obtained in the buckling analysis.

[a]Percentage magnitude of imperfection.
[b]Scale factors applied to the associated mode shapes

4.3.2 Imperfection Sensitivity

In the eigenvalue buckling analysis, calculations gave eigenmodes as shown in Figure 4.1 for all meshes. This showed that the meshing did not affect the perturbation state in extracting the mode shape.

Several analyses were conducted to investigate the maximum amplitude of the wrinkles resulting from different combinations of mode shapes and different scale factors, namely 0.1, 1 and 10%. The results of these combinations were then compared and are summarised in Table 4.2.

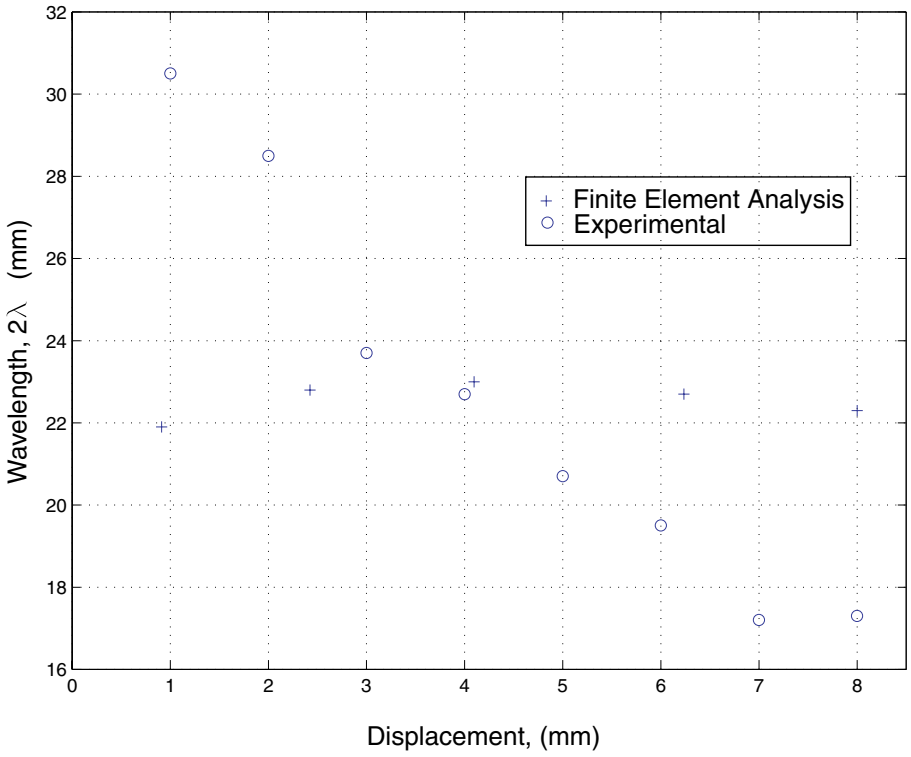

Figure 4.7: Comparison between wavelength obtained from experiment and finite element analysis for Mylar membrane.

With the maximum amplitude values in the range of 2.3–2.5 mm, we can conclude that the structure was not sensitive to the magnitude of the imperfections. Hence, an imperfection of 10% was seeded to perturb the mesh in the analysis. Due to this high level of imperfection, the response of the structure to wrinkling grew steadily before the critical load was reached, hence a smooth transition path to post-wrinkled was obtained and facilitated the analysis.

4.3.3 Comparison to Mansfield Model

The shearing of a membrane strip is a classic problem in tension field theory. The relationship between displacements, u and v, and the orientation of the tension rays, α, in the membrane has been derived. The fundamental equations of the theory are given in Section 1.3.1. Consider a semi-infinite strip which undergoes a constant displacement, u_0, at its upper edge as shown in Figure 4.8.

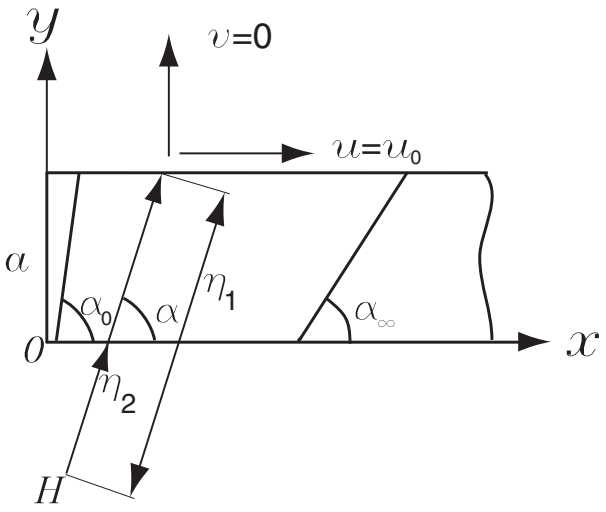

Figure 4.8: Boundary conditions used to determine the function, F.

The boundary conditions are:

$$v = 0, \qquad u = u_0 \tag{4.3}$$

The following equations can be obtained by referring to Figure 4.8:

$$\begin{aligned} \triangle\alpha &= u_0 \cos\alpha \\ \eta_1 - \eta_2 &= a \operatorname{cosec}\alpha \\ \eta_x = \eta_2 &= -\frac{\mathrm{d}x}{\mathrm{d}\alpha}\sin\alpha \end{aligned} \tag{4.4}$$

The negative sign for $\mathrm{d}x/\mathrm{d}\alpha \sin\alpha$ occurs because the locus point H lies below the membrane strip, $\therefore \eta_1 > \eta_2$. From Equation (1.4) and the conditions in Equation (4.4), we can obtain

$$F \propto \frac{\triangle_\alpha^2}{\ln\left(\frac{\eta_1}{\eta_2}\right)} \propto \frac{\cos^2\alpha}{\ln\left(1 - \frac{a\,\mathrm{cosec}^2\,\alpha}{x'}\right)} \tag{4.5}$$

Introducing

$$\mu = \frac{\eta_1}{\eta_2} = 1 - \frac{a\,\mathrm{cosec}^2\,\alpha}{x'} \tag{4.6}$$

we find that $\mu \geq 1$ since x' is always negative in this case. Substitute into Equations (4.4) and (4.5), recall Equation (1.7) to obtain

$$\sin^2\alpha = C\mu(\frac{\ln\mu}{\mu - 1})^2 \tag{4.7}$$

where C is a constant of integration. This constant has a value of 1 when $x \to \infty$ and the tension rays become parallel ($\mu \to 1$ and $\alpha = 45°$). Then, the relation between α and x can be obtained by integration

$$x = a\int_\alpha^{\alpha_o} \frac{\mathrm{cosec}^2\alpha}{\mu(\alpha) - 1}\mathrm{d}\alpha \tag{4.8}$$

A plot of tension ray lines at every 5° with constant stress at the edges is reproduced from Mansfield's model (Mansfield, 1968) based on Equations (4.5)–(4.8). This is compared to the tension rays obtained in the FE analysis using the shell model by introducing geometrical imperfections to the perturbed mesh from the predicted wrinkling mode shapes.

Figure 4.9 shows the tension rays obtained from the finite element analysis and labelled (a)–(e). They are represented by broken lines and superimposed on the tension lines reproduced from the theoretical model. The comparison is shown in Figure 4.10. Note that the tension lines tend to become parallel to each other as they approach infinite length and that α_∞ lies at 45°.

Results obtained from the analysis agreed with the assumptions made in the theory. It was assumed that the stress distribution in the membrane is uniform in the region where α is approaching 45°. It can be seen in Figure 4.6 that the major principal stress distribution is fairly uniform and the minor principal stress is approaching zero in wrinkled region. The orientations of the tension rays, α obtained in the FE analysis lie between 64° to 45°. This is within the limit which requires $\alpha_0 = 90°$ and $\alpha_\infty = 45°$ for the analytical solution in the tension field theory to be valid. Therefore, the analytical model may be used to test the FE shell model.

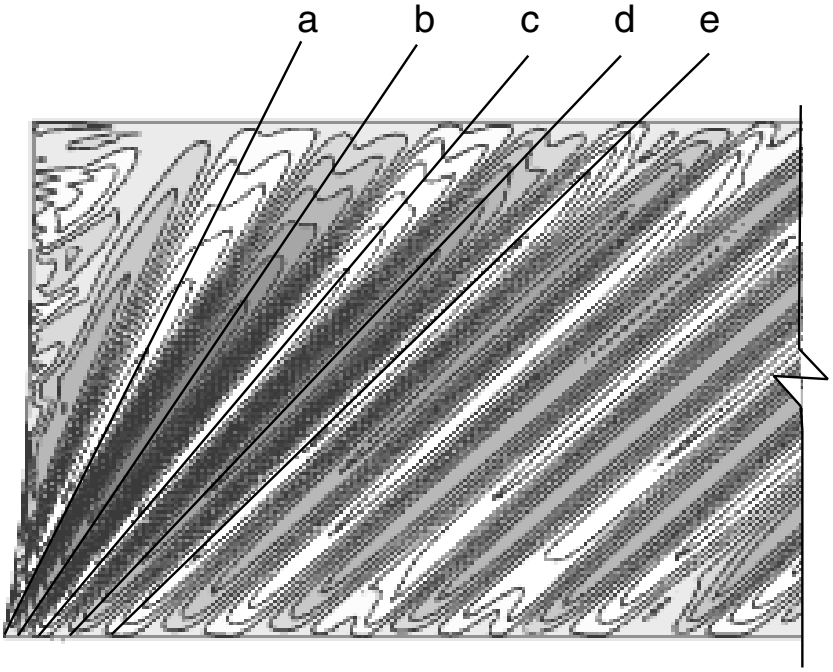

Figure 4.9: Tension ray lines from FE analysis.

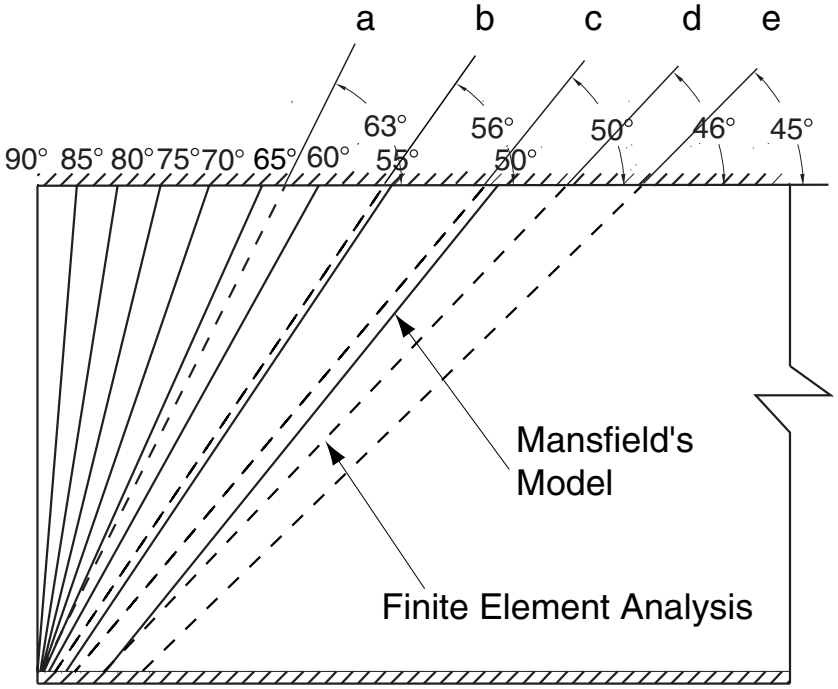

Figure 4.10: Comparison of tension ray lines from Mansfield (1968) and FE model.

We have used a classic problem to verify the procedure described in Section 4.1 for wrinkling analysis. However, when this procedure was extended to analyse the problem presented in Section 3.2, no valid results were obtained. The model became unstable in the eigenvalue buckling analysis stage and an excessive number of negative eigenvalues resulted in solution divergence. This may be due to the boundary conditions not being as well defined in the previous example or there may be a limitation on this analysis method for a partly wrinkled membrane. This is an important subject for further investigation.

Chapter 5

Analytical Solution

The stress state in a highly wrinkled membrane subjected to shear is mainly comprised of tension rays at 45° (Mansfield, 1989). Tension field theory can be used to determine the tension rays in detail. According to this theory there will be an infinite number of wrinkles since the membrane is assumed to have no bending stiffness. Obviously the number of wrinkles is finite and indeed this has been observed in experiments (Rimrott and Cvercko, 1985), hence a small compressive stress need to be allowed to occur. A simple analytical solution to estimate the wavelength of the wrinkle has been developed, based on the experimental observations. This solution assumes that tension rays occur at 45° and that there is a compressive stress equal to the buckling stress, acting perpendicular to the wrinkles.

5.1 Analysis

Let us consider a long, flat isotropic thin elastic sheet of width H clamped to rigid upper and lower edges, as shown in Figure 5.1. When the upper edge is given a small displacement, the material undergoes shear through a small angle, γ. Hence, the overall strain in directions 1 and 2 is $\pm\gamma/2$.

However, when wrinkles occur, if one considers only the elastic deformation of the material due to a uniform uniaxial tensile stress in direction 1, plane stress theory gives

$$\sigma_1 = \sigma, \qquad \sigma_2 = 0 \tag{5.1}$$

this gives the corresponding strains

$$\epsilon_1 = \frac{\sigma}{E} = \frac{\gamma}{2} \tag{5.2}$$

$$\epsilon_2 = -\nu\frac{\sigma}{E} \tag{5.3}$$

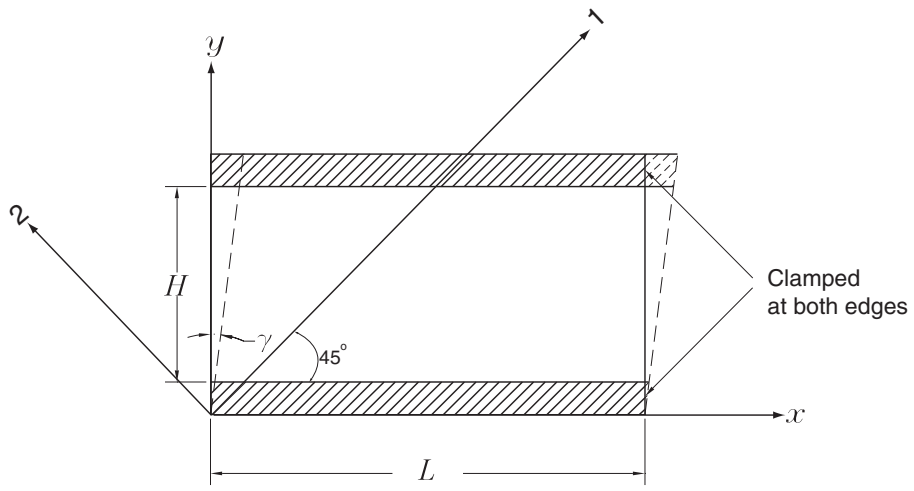

Figure 5.1: Long, flat isotropic membrane clamped to rigid upper and lower edges

Thus, there is a mis-match between strains in direction 2, therefore a "geometric strain" taken by wrinkles has to be introduced. From the above relationships:

$$\text{material strain in direction 2, } \epsilon_{m2} = -\nu\frac{\sigma}{E} = -\nu\frac{\gamma}{2} \tag{5.4}$$

$$\text{overall strain in direction 2, } \epsilon_{o2} = -\frac{\gamma}{2} \tag{5.5}$$

$$\text{geometric strain, } \epsilon_{g2} = -\frac{\gamma}{2}(1-\nu) \tag{5.6}$$

Consider a rectangular membrane of dimensions L and B, subjected to in-plane uniform forces per unit length, N_x, N_y, as shown in Figure 5.2.

Consider w, a small out-of-plane displacement of the membrane. Assuming that

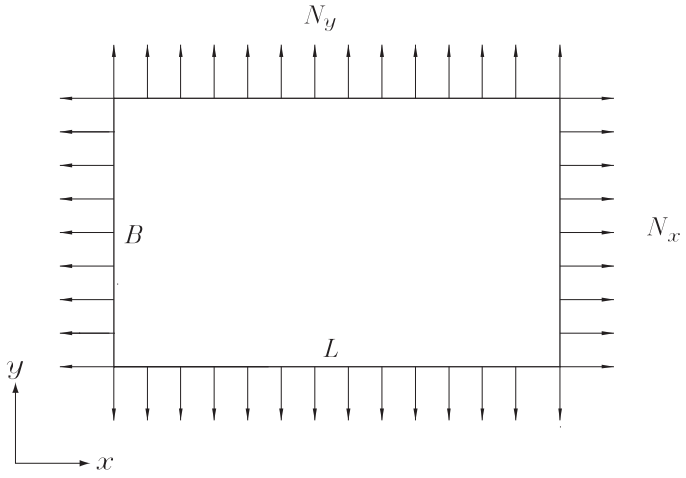

Figure 5.2: Membrane subjected to uniform forces at edges.

the in-plane forces remain approximately constant, the equilibrium equation of the deformed surface in the normal direction is given by (Calladine, 1983)

$$-N_x \frac{\partial^2 w}{\partial x^2} - N_y \frac{\partial^2 w}{\partial y^2} = p_S \tag{5.7}$$

Here the change of curvature is given in terms of the normal displacement, w

$$\kappa_x = \frac{\partial^2 w}{\partial x^2} \tag{5.8}$$

$$\kappa_y = \frac{\partial^2 w}{\partial y^2} \tag{5.9}$$

If the membrane is modelled as a plate the governing equation is

$$D\nabla^4 w = p_B \tag{5.10}$$

where D is the flexural rigidity of the plate

$$D = \frac{Et^3}{12(1-\nu^2)} \tag{5.11}$$

The terms p_S and p_B are the pressure loading on the surface carried by membrane and bending actions, respectively.

Because there is no surface loading on our membranes, we have

$$\begin{aligned} p_S + p_B &= 0 \\ -N_x \frac{\partial^2 w}{\partial x^2} - N_y \frac{\partial^2 w}{\partial y^2} &= D\nabla^4 w \end{aligned} \tag{5.12}$$

Equation (5.12) is the governing equation for the plate in its buckled configuration.

Let us suppose that the plate is simply supported at its boundaries. A trial displacement function can be written as

$$w = w_{mn} \sin(\frac{m\pi x}{L}) \sin(\frac{n\pi y}{B}) \tag{5.13}$$

where m, n are wave numbers. Substituting this into Equation (5.12), we find

$$-N_x \left(\frac{m\pi}{L^2}\right)^2 - N_y \left(\frac{n\pi}{B^2}\right)^2 = D\left[\left(\frac{m\pi}{L^2}\right)^2 + \left(\frac{n\pi}{B^2}\right)^2\right]^2 \tag{5.14}$$

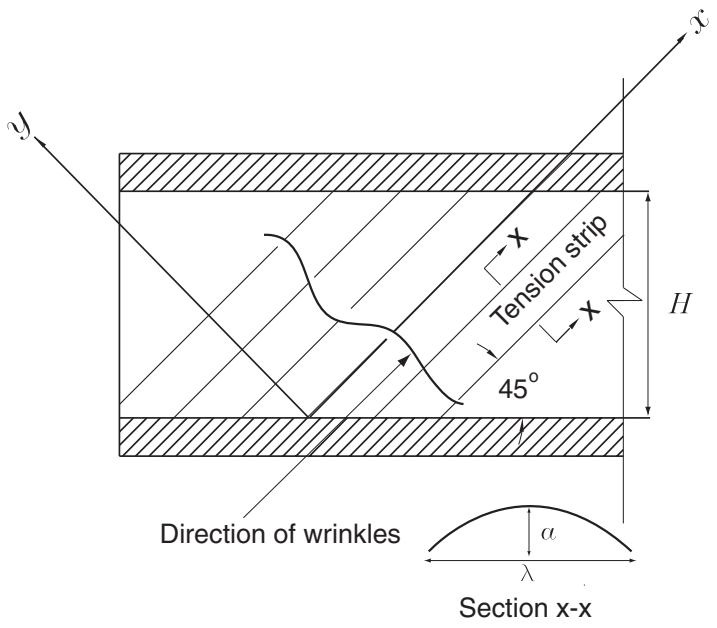

Figure 5.3: Wrinkle pattern in a membrane subjected to pure shear.

5.1.1 Membrane Equilibrium Approach

Reconsider the clamped isotropic membrane in Figure 5.1, subject to shear, and assume that wrinkles form in the direction of the tensile stresses at 45°. Now consider a tension strip whose width coincides with the width λ of a wrinkle, as shown in Figure 5.3.

Let the out-of-plane displacement of the wrinkle be given by

$$w = a \sin \frac{\pi y}{\lambda} \sin \frac{\pi x}{H\sqrt{2}} \tag{5.15}$$

where a is the amplitude, λ is the half wave, i.e. the width of the wrinkle, and the length of the tension strip is equal to $H\sqrt{2}$ as shown in Figure 5.4.

Thus, the tension strip in the wrinkled state has attained a doubly-curved configuration and the principal curvatures, $\kappa_{x,y}$ can be determined from Equations (5.8) and (5.9)

$$\kappa_x = \frac{\pi^2 a}{2H^2} \sin \frac{\pi y}{\lambda} \sin \frac{\pi x}{H\sqrt{2}} \tag{5.16}$$

$$\kappa_y = \frac{\pi^2 a}{\lambda^2} \sin \frac{\pi y}{\lambda} \sin \frac{\pi x}{H\sqrt{2}} \tag{5.17}$$

For the original flat strip to form a wrinkle, a critical transverse compressive stress, σ_{cr} must be reached. This compressive stress is equal to the Euler buckling

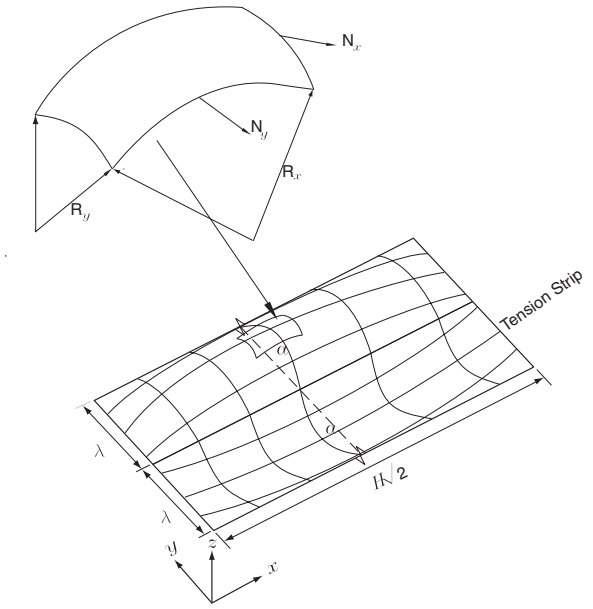

Figure 5.4: Equilibrium state in a tension strip

stress of an infinitely wide plate of length λ. Substituting Equation (5.14), letting m, $n = 1$, and only considering N_y (since this is a calculation for unit width of strip),

$$\begin{aligned} N_y &= -D\frac{\pi^2}{\lambda^2} \\ \therefore\ t\sigma_y &= -\frac{\pi^2}{\lambda^2}\frac{Et^3}{12(1-\nu^2)} \qquad (5.18) \\ \sigma_{\text{cr}} &= \sigma_y = -\frac{\pi^2}{\lambda^2}\frac{Et^2}{12(1-\nu^2)} \qquad (5.19) \end{aligned}$$

The stress σ_x parallel to the wrinkle can be obtained from Equation (5.2)

$$\sigma_x = E\epsilon = E\frac{\gamma}{2} \qquad (5.20)$$

To maintain equilibrium, see Figure 5.4, we use the static equilibrium equation of the membrane. Substituting Equations (5.16), (5.17), (5.19) and (5.20)

$$\begin{aligned} \sigma_x\kappa_x + \sigma_y\kappa_y &= 0 \\ \frac{\pi^2}{\lambda^2}\frac{Et^2}{12(1-\nu^2)}\frac{\pi^2 a}{\lambda^2}\sin\frac{\pi y}{\lambda}\sin\frac{\pi x}{H\sqrt{2}} &= E\frac{\gamma}{2}\frac{\pi^2 a}{2H^2}\sin\frac{\pi y}{\lambda}\sin\frac{\pi x}{H\sqrt{2}} \qquad (5.21) \end{aligned}$$

for which we obtain an expression for the wavelength

$$\lambda^4 = \frac{\pi^2 t^2 H^2}{3(1-\nu^2)\gamma} \qquad (5.22)$$

5.1.2 Strain Energy Approach

An alternative approach using strain energy was proposed by Professor C. R. Calladine and is presented in this section.

The displacement, w, and changes of elastic curvature, $\kappa_{x,y}$, are given by Equations (5.15)–(5.17) as before. First, consider the bending strain energy per unit area, U_B (Calladine, 1983) primarily due to bending in the transverse direction of a wrinkle in Figure 5.3, i.e. the y-direction.

$$U_B = \frac{1}{2} D \kappa_y^2 = \frac{Et^3}{12(1-\nu^2)} \frac{\kappa_y^2}{2} \tag{5.23}$$

The average value is

$$\overline{U}_B = \frac{Et^3}{12(1-\nu^2)} \frac{1}{4} \frac{\pi^4 a^2}{\lambda^4} \tag{5.24}$$

where $\pi^4 a^2 / 4\lambda^4$ is the average strain due to transverse bending.

Now, consider the stretching strain energy per unit area, U_S in the x-direction and neglecting the strain energy in the direction perpendicular to the wrinkles, this is given by

$$U_S = \frac{Et}{2} \epsilon_1^2 \tag{5.25}$$

The principal strain in the x-direction, ϵ_1 is the strain in Equation (5.2) plus the out-of-plain strain

$$\epsilon_1 = \frac{\gamma}{2} + \frac{\pi^2 a^2}{4(H\sqrt{2})^2} \sin^2 \frac{\pi y}{\lambda} \tag{5.26}$$

When $\sin \pi y / \lambda = 1$, we get

$$\begin{aligned} \epsilon_1 &= \frac{\gamma}{2} + \frac{\pi^2 a^2}{8H^2} \\ U_S &= \frac{Et}{2} \left[\left(\frac{\gamma}{2} \right)^2 + \frac{\gamma \pi^2 a^2}{8H^2} + \left(\frac{\pi^2 a^2}{8H^2} \right)^2 \right] \\ &\approx \frac{Et}{2} \frac{\gamma^2}{4} + \frac{Et}{2} \frac{\gamma \pi^2 a^2}{8H^2} \end{aligned} \tag{5.27}$$

The first strain energy term is due to the in-plane shearing of the membrane and the second term is the extra strain energy due to wrinkling. Also note that the third term in the energy is neglected, based on the assumption that $\pi^2 a^2 / 8H^2 \ll \gamma / 2$.

Hence, the total mean strain energy of wrinkling per unit area, including the extra longitudinal strain from Equation (5.27) and the transverse bending strain from Equation (5.24) is

$$U_{\text{wrin}} = \frac{Et}{2}\frac{\gamma\pi^2 a^2}{8H^2} + \frac{Et^3}{12(1-\nu^2)}\frac{\pi^4 a^2}{4\lambda^4} \tag{5.28}$$

The geometric shortening of a sine wave is

$$\epsilon_g = -\frac{\pi^2 a^2}{4\lambda^2} \tag{5.29}$$

where the negative sign represents shortening.

Relating Equation (5.6) to Equation (5.29),

$$\frac{\gamma}{2}(1-\nu) = \frac{\pi^2 a^2}{4\lambda^2} \tag{5.30}$$

Writing λ in term of a,

$$a^2 = \frac{2\gamma(1-\nu)\lambda^2}{\pi^2} \tag{5.31}$$

and substituting this into Equation (5.28),

$$\begin{aligned} U_{\text{wrin}} &= \frac{Et}{2}\frac{\gamma\pi^2}{8H^2}\frac{2\gamma(1-\nu)\lambda^2}{\pi^2} + \frac{Et^3}{12(1-\nu^2)}\frac{\pi^4}{4\lambda^4}\frac{2\gamma(1-\nu)\lambda^2}{\pi^2} \\ &= \frac{\gamma}{8}(1-\nu)Et\left[\frac{\gamma\lambda^2}{H^2} + \frac{\pi^2}{\lambda^2}\frac{t^2}{3(1-\nu^2)}\right] \end{aligned} \tag{5.32}$$

Minimising the terms in brackets with respect to λ we get

$$\lambda^4 = \frac{\pi^2 t^2 H^2}{3(1-\nu^2)\gamma} \tag{5.33}$$

This solution is identical to Equation (5.22), which is not surprising because the two approaches are essentially based on the same assumptions. Once the wavelength of a wrinkle has been determined it is possible to obtain other wrinkle parameters from simple geometric considerations. This method is discussed in the next section.

5.1.3 Prediction of Wrinkle Parameters

Wrinkle Half Wavelength

The half wavelength, λ can be obtained from Equation (5.22) or (5.33)

$$\lambda = \frac{\sqrt{\pi}}{[3(1-\nu^2)]^{\frac{1}{4}}}\frac{\sqrt{Ht}}{\gamma^{\frac{1}{4}}} \tag{5.34}$$

Amplitude

The principal radius, R_y in the transverse direction of the wrinkle, as shown in Figure 5.4, can be determined by

$$R_y = \frac{1}{2}\left(\frac{\lambda^2}{4a} + a\right) \tag{5.35}$$

The maximum amplitude occurs at $y = \lambda/2$ and $x = H\sqrt{2}/2$. Equating Equations (5.17) to (5.35)

$$\kappa_y = \frac{1}{R_y} \tag{5.36}$$

$$\frac{\pi^2 a}{\lambda^2} = \frac{8a}{\lambda^2 + 4a^2}$$

$$a^2 = \frac{7\lambda^2}{4\pi^2}$$

$$a = \frac{\sqrt{7}\lambda}{2\pi} \tag{5.37}$$

5.2 Comparison with Experiments Results

Calculations and measurements of the wavelength for three different materials were compared to verify the relationship between the displacement and wrinkle wavelength developed in Equation (5.34). The materials used were: Kapton membrane of thickness 0.035 mm; Mylar membrane of thickness 0.05 mm; and rubber membrane of thickness 1 mm. Wavelengths were taken in the experiments described in Section 2.3.

In the experiments, the wavelength of the wrinkles in the membrane was recorded for 1 mm increments of shear displacement of the upper edge of the frame, for both thin Kapton and Mylar membrane[1]. The wavelength for the rubber membrane was recorded at every 5 mm intervals. Three wavelengths[2], were measured for each displacement increment and the average values were calculated and plotted.

For the analytical results based on Equation (5.34), the wavelength of a wrinkle is a function of the thickness t, width of membrane H, Poisson's ratio, ν and the shearing angle, γ.

The wavelengths measured in the experiments, the average values and the values calculated using the analytical solution are given in Tables 5.1–5.3 for all three materials. The wavelengths are plotted against the top edge displacement in Figures 5.5–5.7. Wrinkle amplitudes for all three materials calculated using

[1]Small increments needed since these membranes are assumed to be inextensional.

[2]Only two for rubber membrane.

Displacement (mm)	Experimental (mm)				Analytical (mm)
	$2\lambda_1$	$2\lambda_2$	$2\lambda_3$	$2\lambda_{ave}$	2λ
1	25.0	26.0	24.5	25.2	23.4
2	20.0	21.0	18.5	19.8	19.7
3	18.5	19.0	19.0	18.8	17.8
4	18.0	18.5	18.0	18.2	16.6
5	17.5	18.2	17.0	17.6	15.7
6	16.0	18.0	15.0	16.3	15.0
7	14.0	13.5	16.0	14.5	14.4
8	15.0	13.0	14.0	14.0	13.9

Table 5.1: Experimental and analytical results for Kapton membrane of thickness 0.035 mm.

Equation (5.37) and those measured in the experiment with the corresponding displacements are also compared and presented in Table 5.4.

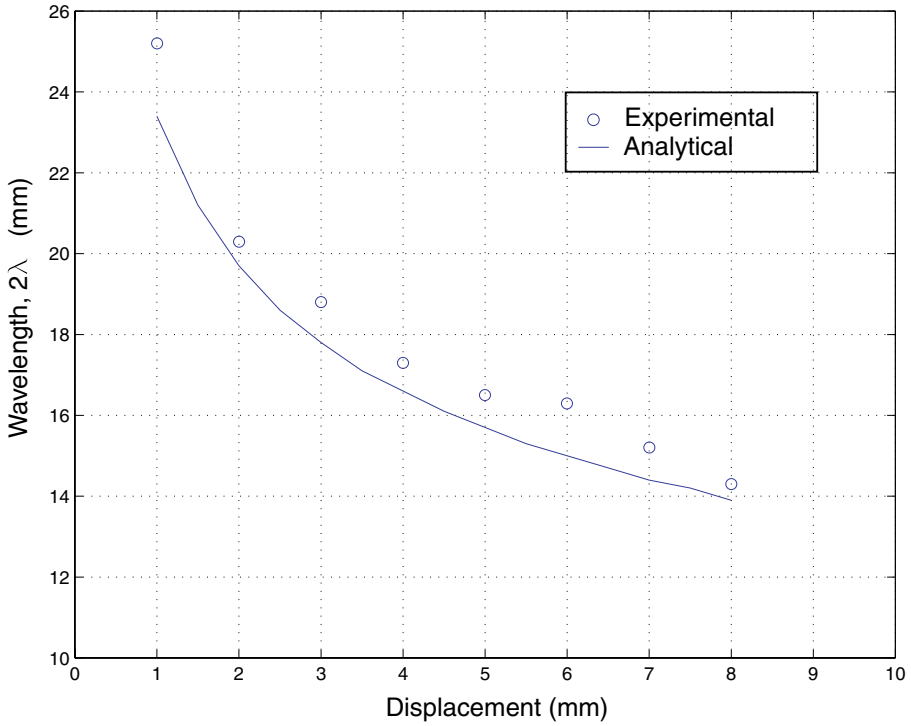

Figure 5.5: Comparison between experimental and analytical solution for Kapton membrane.

Displacement (mm)	Experimental (mm)				Analytical (mm)
	$2\lambda_1$	$2\lambda_2$	$2\lambda_3$	$2\lambda_{ave}$	2λ
1	30.0	30.5	31.0	30.5	28.0
2	29.0	28.0	28.5	28.5	23.5
3	25.0	22.0	24.0	23.7	21.3
4	23.0	21.0	24.0	22.7	19.8
5	20.0	22.0	20.0	20.7	18.7
6	20.5	19.9	19.9	19.5	17.9
7	17.5	17.0	17.0	17.2	17.2
8	18.0	17.0	17.0	17.3	16.6

Table 5.2: Experimental and analytical results for Mylar membrane of thickness 0.05 mm.

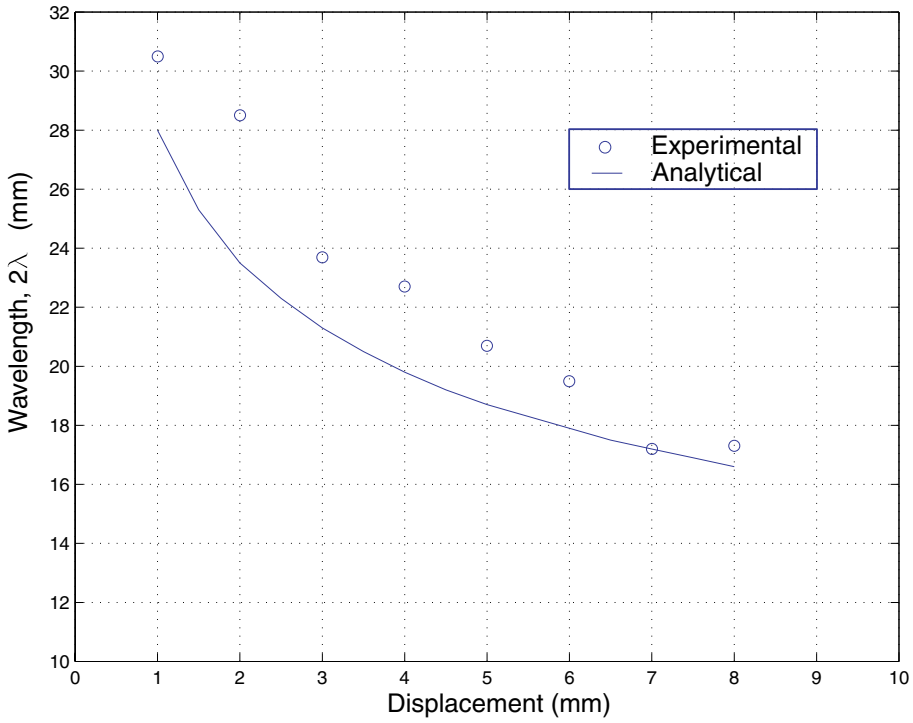

Figure 5.6: Comparison between experimental and analytical solution for Mylar membrane.

Displacement (mm)	Experimental (mm)			Analytical (mm)
	$2\lambda_1$	$2\lambda_2$	$2\lambda_{ave}$	2λ
5	75.0	75.0	75.0	81.7
8	71.0	71.0	71.0	73.8
10	70.0	71.0	70.5	68.7
15	69.0	70.0	69.5	62.1
20	65.0	65.0	65.0	57.8
25	64.0	64.0	64.0	54.6
30	62.0	62.0	62.0	52.2
35	60.0	60.0	60.0	50.2
40	56.0	57.0	56.5	48.6
45	55.0	55.0	55.0	47.2
50	55.0	55.0	55.0	45.9

Table 5.3: Experimental and analytical results for a rubber membrane of thickness 1 mm.

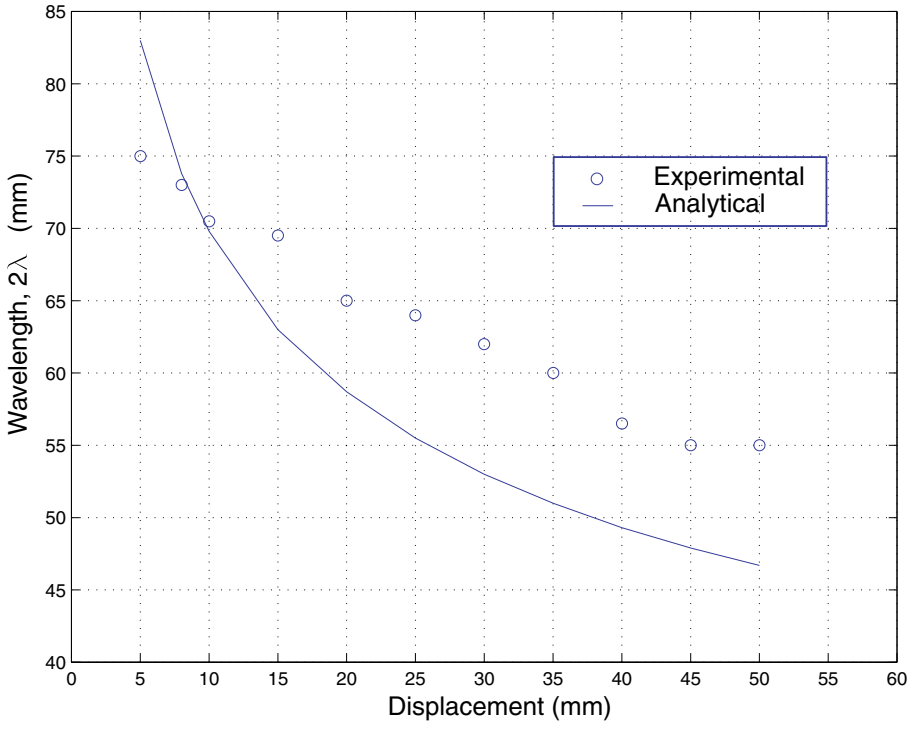

Figure 5.7: Comparison between experimental and analytical solution for Rubber membrane.

Material	Displacement (mm)	Amplitude (mm)	
		Experimental	Analytical
Kapton	8	2.5	2.9
Mylar	8	3.0	3.6
Rubber	20	12.0	13.7

Table 5.4: Comparisons between experimental and analytical solution for three materials.

5.3 Discussion

Generally the estimated wavelength using Equation (5.34) is approximately 8% lower than the value obtained in the experiments. However, the variation in wavelength and shearing angle appears to be predicted well by

$$\lambda \propto \frac{1}{\gamma^{\frac{1}{4}}} \tag{5.38}$$

This implies that the wavelength is almost constant after reaching certain displacement. This relationship is checked by plotting the experimental results into log scale as shown in Figure 5.8. The results obtained for three materials produced approximately the same gradient as in the 1/4 line plotted as a reference line, hence Equation (5.38) is verified. γ is assumed to be small in the calculation, which may explain why the error for the rubber membrane was 5% greater than in the stiffer membranes which were subjected to only small displacements. This small angle assumption might have been violated for rubber. The actual strain used in Equation (5.20) should be referred to the longitudinal strain, ϵ_x along the wrinkle. Instead, the calculation was based on the shear strain, since the strain is small we have assumed that the differences are negligible.

Also, we have assumed that there is no initial prestress. If an initial prestress, σ_o is introduced, Equation (5.19) should be rewritten as

$$\sigma_{\text{cr}} = \sigma_y - \sigma_o \tag{5.39}$$

The other possible explanation of the discrepancy between the theory and the results observed in the experiment may be due to the assumption that wrinkles form at 45°. It was observed in the experiment that not all tension rays were at 45° and they were not always parallel to each other.

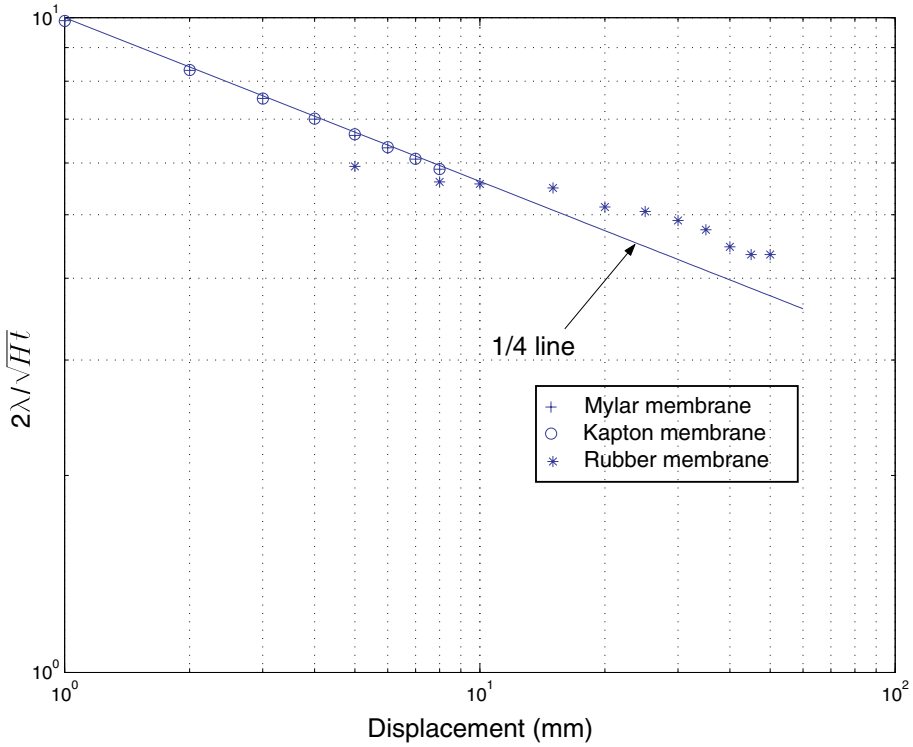

Figure 5.8: Plot to verify the relationship between wavelength and displacement.

Chapter 6

Conclusions

The main objective of this dissertation was to develop analytical tools to study the wrinkling which is often found in thin prestressed membrane structures. Wrinkle patterns and their parameters were of most interest in the analysis since the behaviour and performance of these structures can be adversely affected by their occurrence. The main achievements in the study are now discussed and summarised, together with the future work that is needed.

6.1 Discussion

6.1.1 Use of Finite Elements in Wrinkling Analysis

Two different finite element methods were used to analyse wrinkling in a prestressed membrane. Different loading conditions and boundary conditions were considered. Two theories were employed to analyse the wrinkling problem.

It has been shown that both theories, i.e. wrinkling theory and buckling theory, once they have been incorporated into a commercial finite element code, are able to simulate the wrinkling condition reasonably well.

In the first method wrinkling theory was used. The wrinkled membrane was simulated as a membrane in which compressive stresses were not allowed to be developed. We were able to predict the in-plane wrinkle pattern but with no information about the out-of-plane deformation. This method can predict the wrinkle regions and the wrinkle patterns reliably.

However, if the out-of-plane deformation is of interest, then the results obtained from the in-plane analysis need to be processed further and a post-processing subroutine was written to estimate the wrinkle parameters. For this purpose, it is useful to have some previous experimental observations available, as these help

to identify the size and shape of the wrinkled region in the membrane. The user then defines various boundaries and shapes of the wrinkles.

Slow convergence rate was encountered in this analysis when no-compression material behaviour was assigned to the membrane. This may make the method unsuitable to analyse highly wrinkled membranes. There will be excessive numerical singularities in the solutions and consequently this may cause premature termination of the analysis.

Bifurcation buckling theory was used in the second method. The wrinkling problem was treated as a conventional eigenvalue buckling problem and the corresponding eigenmodes were extracted. This analysis used shell elements which allow compressive stresses to be developed in the membrane. However, no compression or only small compressive stresses[1] were found in the problem we have investigated. This means that the results matched the tension field assumptions.

This analysis is able to determine the precise shape of the wrinkles and hence the out-of-plane deformation can be obtained. However, these parameters, i.e. number of wrinkles and wavelength, were found to be dependent on the mesh density used in the model. There are convergence problems associated with very fine meshes. Therefore, remeshing should be carried out in the wrinkled regions which are specifically needed for measurements, for example in the region whose wavelength is to be measured.

The magnitude of imperfections introduced in the initial mesh was another aspect considered in this analysis. Although the model we used was not sensitive to imperfections, by combining several eigenmode shapes and different magnitude of imperfections we were able to predict and simulate the wrinkles more accurately.

By comparing these two analysis methods, we found that the element mesh density need not be too fine for the in-plane wrinkling analysis used in the first method, since only wrinkle regions and patterns were determined. In the second method in which the wrinkle parameters were determined, required the elements to be smaller than half the wavelength of a wrinkle; hence a very fine mesh was needed. This involved larger analysis time versus resolutions of the wrinkles which made the computation expensive. This can be compared to the first analysis, which required a preliminary scale model to be set up in order to determine the out-of-plane deformations.

6.1.2 The Analytical Approach

Particular attention was given to the development of an analytical solution to predict the wrinkle wavelength, this was mainly due to its relation to the amplitude of the wrinkles formed. This information is particularly important for

[1] Relative to the tensile stresses.

structures which require a highly accurate surface.

Several assumptions are made in this approach:

1. The stress distribution in the wrinkled region is uniform and all wrinkles are formed at 45°.
2. The critical wrinkling stress in the transverse section of a wrinkle is equivalent to the buckling stress of a this plate with the properties of the membrane, hence the membrane possesses small bending stiffness.
3. A wrinkle is a strip which has taken a doubly curved configuration that can be described by a half sine wave.
4. The membrane is isotropic and the principal radius of curvature and thickness are assumed to be constant over a wide region of the sheet. There is no out-of-plane displacement at the edges of the wrinkled strip.

Two approaches using the static membrane equilibrium and strain energy have been used to determine the wavelength based on the above assumptions. The solutions obtained agreed with each other. The wavelength of the wrinkle was found to be a function of the membrane dimensions, i.e. thickness and width of the membrane, also, the displacement applied and the material used.

6.2 Future work

As work was progressing to develop more reliable tools to analyse wrinkling, several improvements have been identified. These are outlined in this section.

For FE wrinkling analysis using wrinkling theory, only the principal stress wrinkling criterion was employed in the no-compression material. The other two criteria reviewed in Section 1.3.5 may need to be considered for comparison. A program could be developed using the user-defined subroutine *UMAT in ABAQUS, to define the material's mechanical behaviour. Therefore, different convergence criteria can be redefined and implemented for the membrane elements. This change may also improve the slow convergence rate encountered in the analysis.

The procedures may need to be tested on membranes with more complicated shapes, e.g. Collapsible Rib Tension Surface (CRTS) antenna reflector (Rits, 1996) and NGST solar shield, all subjected to non-uniform loading. Wrinkle patterns in a membrane in static and dynamic states may be a possible area of research.

As for eigenvalue buckling analysis, further investigation on the relationship between the wavelength and the displacement in the model subjected to pure shear

is necessary, in order to achieve better agreement with the results obtained from the experimental observations and analytical solution. The analysis should be extended to model membranes with different loading conditions and boundary conditions. Analysis of a partly wrinkled membrane needs to be implemented.

The assumptions made in the analytical approach, e.g. uniform stress in wrinkled region, and the incompatibility of the solution at the edges, etc. may need to be modified and improved. Also, the exact relationship between wavelength and the longitudinal strain along the wrinkle and the range of the "small angle" for this approach to work well may need to be identified. The analytical solution method could be included in the post-processing subroutine written to predict the out-of-plane deformation in the 2-D analysis.

Finally, a more accurate experiment with a larger membrane test specimen is required to verify the numerical analysis. This should include accurate measurements of various wrinkle parameters and also the stress levels in the membrane.

Bibliography

ABAQUS (1994). ABAQUS/Answers. *ABAQUS News Letter, Answers to Common ABAQUS Questions*, Winter issue(5).

ABAQUS (1998). *User's Manual Version 5.8.* Hibbit Karlson and Sorensen Inc.

Adler, A. L., Mikulas, M. M., and Hedgepeth, J. M. (2000). Static and Dynamic Analysis of Partially Wrinkled Membrane Structures. *41st AIAA/ASME/ASCE/AHS/ASC Structures, Structures Dynamics, and Material Conference and Exhibit.* Atlanta, GA. AIAA-2000-1810.

Allen, H. G. and Bulson, P. S. (1980). *Background to Buckling.* McGraw-Hill Book Compony(UK) Limited, England.

Bernasconi, M. C. and Rits, W. J. (1990). Inflatable, Space-Rigidised Support Structures for Large Spacebourne Optical Interferometer Systems. *Acta Astronautica*, 22:145–153.

Calladine, C. R. (1983). *Theory of Shell Structures.* Cambridge University Press, Cambridge.

Contri, P. and Schrefler, B. A. (1988). A Geometrically Nonlinear Finite Element Analysis of Wrinkled Membrane Surfaces by A No-compression Material Model. *Communications in Applied Numerical Methods*, 4:5–15.

Ewins, D. J. (1995). *Model Test: Theory and Practice.* Research Studies Press Ltd., England, Ninth edition.

Greschik, G., Mikulas, M. M., and Freeland, R. E. (1998). Scaling of Nonlinear Phenomena with Emphasis on Thin Film Deployable Structures. *Symposium on Deployable Structures: Theory and Application, Cambridge, UK.*

Greschik, G., Mikulas, M. M., and Palisoc, A. (2000). Torus-Less Inflated Membrane Reflector with an Exact Parabolic Center. *41st AIAA/ASME/ASCE/AHS/ASC Structures, Structures Dynamics, and Material Conference and Exhibit.* Atlanta, GA. AIAA-2000-1810.

Grossman, G. (1998). Analysis of Rim Supports for Off-axis Inflatable Reflector. I&II. *Journal of Aerospace Engineering*, 4:47–77.

Kang, S. and Im, S. (1997). Finite Element Analysis of Wrinkling Membranes. *Journal of Applied Mechanics*, 64:263–269.

Kato, S. (1988). Concept of Inflatable Elements Supported by Truss Structures for Reflector Application. In *Proc. 39th Cong. of the International Astronautical Federation*. Bangalore, India.

Kato, S. (1989). Research and Development of a Reflector Structure Employing Inflatable Elements. In *Proc. 40th Cong. of the International Astronautical Federation*. Malaga, Spain.

Lai, C. Y. (1997). Shape and Stress Analysis of Edge-tensioned Membranes. MPhil Thesis, University of Cambridge.

Liu, X., Jenkins, C. H., and Schur, W. W. (1998). Computation Issues in the Modelling of Wrinkling During Parachute Deployment. *Symposium on Deployable Structures: Theory and Application, Cambridge, UK*.

Mansfield, E. H. (1968). Tension Field Theory, a new approach which shows its duality with inextensional theory. *Proc. XII Int. Cong. Appl. Mech.*, pages 305–320.

Mansfield, E. H. (1970). Load Transfer via a Wrinkled Membrane. *Proc. Roy. Soc. Lond. A.*, 316:269–289.

Mansfield, E. H. (1989). *The Bending and Stretching of Plates*. Cambridge University Press, Cambridge, Second edition.

MATLAB (1993). *Reference Guide*. The. Maths. Works Inc.

Mikulas, M. M. (1964). Behavior of A Flat Stretched Membrane Wrinkled by The Rotation of An Attached Hub. Master's thesis, Virginia Polytechnic Institute.

Miller, R. K. and Hedgepeth, J. M. (1982). An Algorithm for Finite Element Analysis of Partly Wrinkled Membranes. *AIAA*, 20:1761–1763.

Miller, R. K., Hedgepeth, J. M., Weingarten, V. I., Das, P., and Kahyai, S. (1985). Finite Element Analysis of Partly Wrinkled Membranes. *Computers and Structures*, 20:631–639.

Miyamura, T. (2000). Wrinkling of Stretched Circular Membrane under In-Plane Torsion: Bifurcation Analyses and Experiments. *Engineering Structures*, 20:1407–1425.

Murphey, T. M. (1998). *A Two-Dimensional Constitutive Model for Wrinkled Thin Films*. PhD thesis, University of Colorado at Boulder, Center for Aerospace Structures.

Pipkin, A. C. (1986). The Relax Energy Density for Isotropic Elastic Membrane. *IMA Journal of Applied Mathematics*, 36:85–99.

Reissner, E. (1938). On tension field theory. *Proc. V Int. Cong. Appl. Mech.*, pages 88–92.

Rimrott, F. P. J. and Cvercko, M. (1985). Wrinkling in Thin Plates Due to In-Plane Body Forces. *Inelastic Behaviour of Plates and Shells*. IUTAM Symposium Rio de Janeiro.

Rits, W. J. (1996). A Multipurpose Deployable Membrane Reflector. *ESA Bulletin*, 88:66–71.

Stein, M. and Hedgepeth, J. M. (1961). Analysis of Partly Wrinkled Membranes. *NASA TN D-813*.

Wagner, H. (1929). Flat Sheet Metal Girder with Very Thin Metal Web. *Zeitschrift für Flugtechnik Motorlurftschiffahrt*, 20.

Watt, A. M. (2000). Lightweight Deployable SAR Structures. MPhil Thesis, University of Cambridge.